Article

The neural basis of species-specific defensive behaviour in *Peromyscus* mice

https://doi.org/10.1038/s41586-025-09241-2

Received: 4 July 2023

Accepted: 4 June 2025

Published online: 23 July 2025

Open access

Check for updates

Felix Baier[1,2,3,4,10,14] ✉, Katja Reinhard[5,6,11,14], Bram Nuttin[5,6], Arnau Sans-Dublanc[5,6], Chen Liu[5,6], Victoria Tong[1,12], Julie S. Murmann[5,13], Keimpe Wierda[7], Karl Farrow[5,6,8,9,15] ✉ & Hopi E. Hoekstra[1,2,3,4,15] ✉

Evading imminent threat from predators is critical for animal survival. Effective defensive strategies can vary, even between closely related species. However, the neural basis of such species-specific behaviours remains poorly understood[1–4]. Here we find that two sister species of deer mice (genus *Peromyscus*)[5] show different responses to the same looming stimulus: *Peromyscus maniculatus*, which occupies densely vegetated habitats, predominantly escapes, whereas the open field specialist, *Peromyscus polionotus*, briefly freezes. This difference arises from species-specific escape thresholds, is largely context-independent, and can be triggered by both visual and auditory threat stimuli. Using immunohistochemistry and electrophysiological recordings, we find that although visual threat activates the superior colliculus in both species, the role of the dorsal periaqueductal grey (dPAG) in driving behaviour differs. Whereas dPAG activity scales with running speed in *P. maniculatus*, neural activity in the dPAG of *P. polionotus* correlates poorly with movement, including during visually triggered escape. Moreover, optogenetic activation of dPAG neurons elicits acceleration in *P. maniculatus* but not in *P. polionotus*, and their chemogenetic inhibition during a looming stimulus delays escape onset in *P. maniculatus* to match that of *P. polionotus*. Together, we trace species-specific escape thresholds to a central circuit node, downstream of peripheral sensory neurons, localizing an ecologically relevant behavioural difference to a specific region of the mammalian brain.

To survive in the wild, animals must respond to external sensory stimuli with actions that are appropriate for their local environment. Variation in behavioural responses may arise through learning or behavioural plasticity, or evolve through heritable changes of the underlying neural circuitry. In the latter case, changes in sensory detection and/or processing have been shown to underlie behavioural evolution (for example, host preference in mosquitos[1] and food preference in birds[3], cockroaches[4] and fruit flies[2]). When known, these sensory changes are most often due to genetic changes in peripheral sensory systems (for example, odour or taste receptors and opsins[6,7], but see ref. 8). By contrast, how evolution modifies central neural circuits to alter the innate behavioural responses of animals is less well understood[9].

Visual stimuli have long been used to study defensive behaviours. A famous example is Tinbergen's recordings of the behaviour of birds exposed to cardboard models of aerial predators[10,11]. This paradigm has since been modified to study naturalistic antipredator response to overhead visual stimuli under controlled conditions[12–19]. In this assay, laboratory mice (genus *Mus*) tend to freeze when exposed to a gliding overhead predator ('sweeping' stimulus), and often flee or escape when exposed to an attacking predator ('looming' stimulus). Robust behavioural responses, such as these, have been used to uncover the underlying neural circuits, including a key role for the superior colliculus in translating visual stimuli into appropriate defensive reactions[20–22], with projections from the retinorecipient superficial superior colliculus (sSC) to, for example, the deep layers of the superior colliculus (dSC) and on to the dPAG[23–27]. Notably, dPAG neurons have been shown to command the initiation of escape actions[27–30].

These defensive behaviours, and the brain regions involved, may diverge in species that have evolved in distinct environments, in which different defensive strategies may be more or less effective[31]. Deer mice (genus *Peromyscus*) occupy diverse habitats across North America[5], including species living in the underbrush of densely vegetated habitats (*P. maniculatus*) or those specialized for life in exposed, open fields with little to no vegetation (*P. polionotus*). Using these two ecologically divergent sister species, we show that they differ in behavioural response to the same visual threat and then identify a locus in the neural circuit where evolution is likely to have acted.

[1]Department of Molecular and Cellular Biology, Harvard University, Cambridge, MA, USA. [2]Department of Organismic and Evolutionary Biology, Harvard University, Cambridge, MA, USA. [3]Museum of Comparative Zoology, Harvard University, Cambridge, MA, USA. [4]Center for Brain Science, Harvard University, Cambridge, MA, USA. [5]Neuro-Electronics Research Flanders, Leuven, Belgium. [6]Department of Biology, KU Leuven, Leuven, Belgium. [7]Electrophysiology Unit, VIB-KU Leuven Center for Brain and Disease Research, CBD Technologies, Leuven, Belgium. [8]VIB, Leuven, Belgium. [9]imec, Leuven, Belgium. [10]Present address: Max Planck Institute for Brain Research, Frankfurt, Germany. [11]Present address: Scuola Internazionale Superiore di Studi Avanzati, Trieste, Italy. [12]Present address: Vanderbilt University School of Medicine, Nashville, TN, USA. [13]Present address: Institute of Science and Technology Austria, Klosterneuburg, Austria. [14]These authors contributed equally: Felix Baier, Katja Reinhard. [15]These authors jointly supervised this work: Karl Farrow, Hopi E. Hoekstra. ✉e-mail: felixsbaier@gmail.com; karl.farrow@kuleuven.be; hoekstra@oeb.harvard.edu

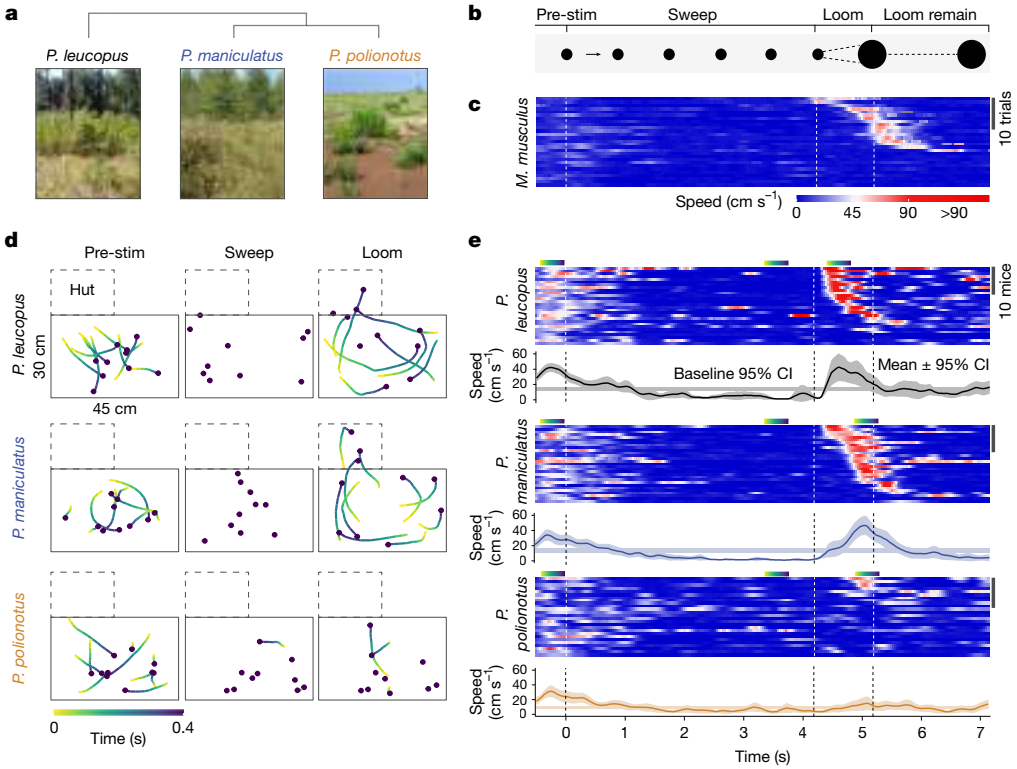

Fig. 1 | Evolution of defensive behaviour in ecologically distinct *Peromyscus* species. a, Phylogenetic relationship of three focal *Peromyscus* species with representative photographs of their natural habitat. Image credit: Aimee Tomcho (*P. leucopus* habitat), Yu Man Lee (*P. maniculatus* habitat), Hopi Hoekstra (*P. polionotus* habitat). **b**, Schematic representation of the sweep–looming stimulus. **c**, Defensive response of *Mus musculus* (C57Bl6 strain) during the sweep–looming stimulus. Rows represent individual trials ($n = 14$ mice, tested twice). Trials are sorted by escape onset during the looming stimulus, with earliest on top. Speed is indicated by a colour gradient. **d**, Representative movement trajectories of individual mice ($n = 10$) of *P. leucopus*, *P. maniculatus* and *P. polionotus* during 0.4 s before stimulus onset (left), during sweeping (middle) and during looming (right). Time is indicated by a colour gradient. **e**, Defensive response of *Peromyscus* species during the sweep–looming stimulus. Rows represent individual mice (*P. polionotus*, $n = 26$; *P. maniculatus*, $n = 29$; *P. leucopus*, $n = 28$). Trials are sorted by escape onset during the looming stimulus, with earliest on top. Speed colour gradient is the same as in **c**. Three bars above each raster plot indicate the time period of the trajectories shown in **d**, and for looming are centred on the peak mean speed of each species. Line plots represent mean speed ± 95% confidence interval (CI); horizontal shaded lines represent the 95% confidence interval of mean speed averaged across the 60 s before stimulus onset.

Species-specific defences in *Peromyscus*

To test whether defensive behaviours differ among animals from distinct habitats, we selected two closely related species of *Peromyscus*: the open field specialist *P. polionotus subgriseus*, and densely vegetated prairie inhabitant, *P. maniculatus bairdii*. A third species, *Peromyscus leucopus*, which is largely sympatric with *P. maniculatus*, was included as an outgroup to determine the lineage in which any observed differences evolved (Fig. 1a). To quantify defensive behaviours, we placed mice in an open arena that included a refuge (a hut; Extended Data Fig. 1a) and measured their response to an overhead 'sweep–looming' stimulus, which resembles an aerial predator searching for (sweep), and then rapidly descending upon (looming), its prey (Fig. 1b). In this assay, laboratory mice decelerated during the sweeping phase of the stimulus and accelerated during its looming phase (Fig. 1c), consistent with previous findings[13]. Similarly, wild-derived, laboratory-born adults of each *Peromyscus* species generally decelerated and largely remained immobile during the sweeping phase of the stimulus (Fig. 1d,e, Extended Data Fig. 1b,c and Supplementary Videos 1 and 2). Conversely, the response during the looming phase of the stimulus revealed marked differences between species (Fig. 1d,e, Extended Data Fig. 1b,c and Supplementary Videos 1 and 2). Both *P. maniculatus* and *P. leucopus* accelerated and ran rapidly across the arena ('escaping'; Extended Data Fig. 1d,e), often towards the refuge. By contrast, the open field specialist, *P. polionotus*, tended to remain immobile ('freezing'; Extended Data Fig. 1d,f). Notably, we did not observe any species-specific differences in behaviour before the onset of the sweep–looming stimulus (Extended Data Fig. 1c). Phylogenetic comparison suggests that freezing in response to a looming stimulus is derived, and therefore the change in defensive response probably evolved along the *P. polionotus* lineage. Because the largest behavioural difference observed was in response to looming (Extended Data Fig. 1d,g,h and Supplementary Videos 3 and 4), we focused on this threat stimulus for subsequent experiments.

Escape thresholds differ between species

With increasing threat intensity, prey animals often switch from immobility to rapid escape[13,32]. To determine whether *P. maniculatus* and *P. polionotus* show similar changes in behaviour, we exposed a new cohort of each species to five repetitions of a looming stimulus that varied in contrast (threat intensity; Fig. 2a and Extended Data Fig. 2a). At low contrast (32%), most individuals of both species froze (16 out of 27 *P. maniculatus* and 28 out of 41 *P. polionotus*), and only a few mice escaped (10 out of 27 *P. maniculatus* and 12 out of 41 *P. polionotus*). As the contrast level increased, the proportion of escaping mice increased in both species, but the rate of change differed between the species (Fig. 2a). For example, at intermediate contrast (72%), most *P. maniculatus* (24 out of 25) but few *P. polionotus* (6 out of 28) escaped, whereas at high contrast (100%), the proportion of mice that escaped was not significantly different between species

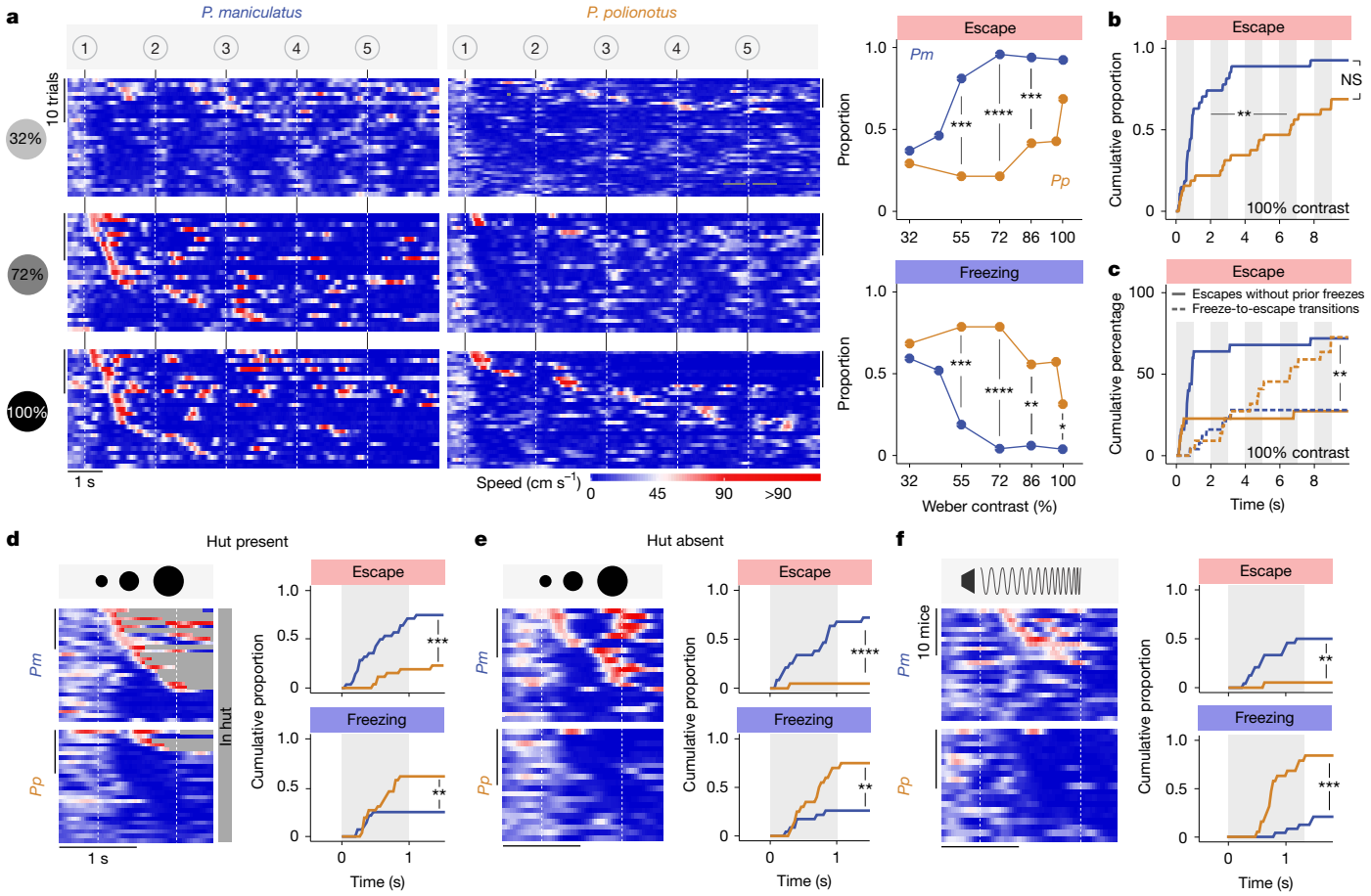

Fig. 2 | Escape threshold differences underlie species-specific behaviour. **a**, Left, behavioural response to five repetitions of visual threat of varying intensity (looming contrast: 32%, 72% or 100%). Rows represent individual mice of *P. maniculatus* (left) and *P. polionotus* (right). Trials are sorted by latency to escape threshold. Right, proportion of individual mice of *P. maniculatus* and *P. polionotus* showing escape (top) and freezing (bottom) across these and additional contrast levels (far right; escape, 32% contrast $P = 0.685$, 55% contrast $P = 4 \times 10^{-4}$, 72% contrast $P = 2 \times 10^{-7}$, 86% contrast $P = 9 \times 10^{-4}$, 100% contrast $P = 0.052$; freezing, 32% contrast $P = 0.615$, 55% contrast $P = 4 \times 10^{-4}$, 72% contrast $P = 2 \times 10^{-7}$, 86% contrast $P = 0.002$, 100% contrast $P = 0.0177$). **b**, Cumulative proportion of individual mice showing escape during 100% contrast looming stimulus (latency, $P = 0.009$; proportion, $P = 0.052$). **c**, Cumulative percentage of escaping mice that either escaped without first freezing (solid line) or that first froze and then transitioned to escape (dashed) ($P = 0.006$). **d**–**f**, Raster plots and cumulative proportion of individual mice showing escape and freezing during a single looming stimulus (100% contrast) in the presence of hut (**d**; escape, $P = 4 \times 10^{-4}$; freezing, $P = 0.007$), in the absence of hut (**e**; escape, $P = 2 \times 10^{-5}$; freezing, $P = 0.009$), and during a sound frequency upsweep (**f**; escape, $P = 0.005$; freezing, $P = 5 \times 10^{-4}$). Two-sided chi-squared test (proportion, cumulative proportion and cumulative percentage), two-sided Kolmogorov–Smirnov test (escape onset distribution). *Pm*, *P. maniculatus*; *Pp*, *P. polionotus*. $^{*}P < 0.05$; $^{**}P < 0.01$; $^{***}P < 0.001$; $^{****}P < 0.0001$; NS, not significant.

(25 out of 27 *P. maniculatus* and 22 out of 32 *P. polionotus*). However, even at high contrast, the onset of escape was significantly delayed in *P. polionotus* (Fig. 2b and Extended Data Fig. 2b), because 73% of *P. polionotus* individuals that eventually escaped initially froze at the onset of the stimulus (Fig. 2c and Supplementary Video 5). Notably, although the proportion of mice that showed a visible behavioural reaction to the detection of the stimulus increased with contrast in both species, and was overall higher in *P. maniculatus* (Extended Data Fig. 2c), the species-specific responses were not different in this subset of individuals (Extended Data Fig. 2d). Moreover, contrast sensitivity curves obtained from single-neuron recordings in the sSC did not differ between the two species (Extended Data Fig. 2f–h), suggesting that a difference in stimulus detection does not explain the species-specific behavioural responses. Together, we find that both species are more likely to freeze at low threat levels and more likely to escape at high threat levels, but that the threat level ('threshold') at which each species switches from freezing to escape differs: *P. maniculatus* transition to escape behaviour at an approximately twofold lower threat intensity than *P. polionotus*.

We next tested whether the availability of a refuge and/or stimulus modality affect the observed differences in defensive behaviour. First, we compared the response to a single looming stimulus of two new cohorts that either had access to a refuge or not. Unlike in laboratory mice[33], the species-specific responses were recapitulated in the absence of the hut (escape with hut: 21 out of 28 *P. maniculatus* and 6 out of 26 *P. polionotus*; escape without hut: 17 out of 23 *P. maniculatus* and 1 out of 20 *P. polionotus*) (Fig. 2d,e), suggesting that they are not driven by differences in the perception of safety afforded by the refuge. Notably, of the mice that escaped after five repetitions of the high-contrast looming stimulus (Fig. 2a–c), the majority of *P. polionotus*, but not *P. maniculatus*, retreated into the hut (63.6% versus 28.0%; Extended Data Fig. 2e), suggesting that *P. polionotus* escape primarily to seek safety in a refuge. To determine whether the observed behavioural differences are specific to visual stimuli, we exposed a new cohort to an aversive ultrasound frequency upsweep[33,34]. Although the auditory stimulus was overall less salient than the visual stimuli, we again observed remarkably similar species-specific behaviour: many *P. maniculatus* accelerated and some escaped (12 out of

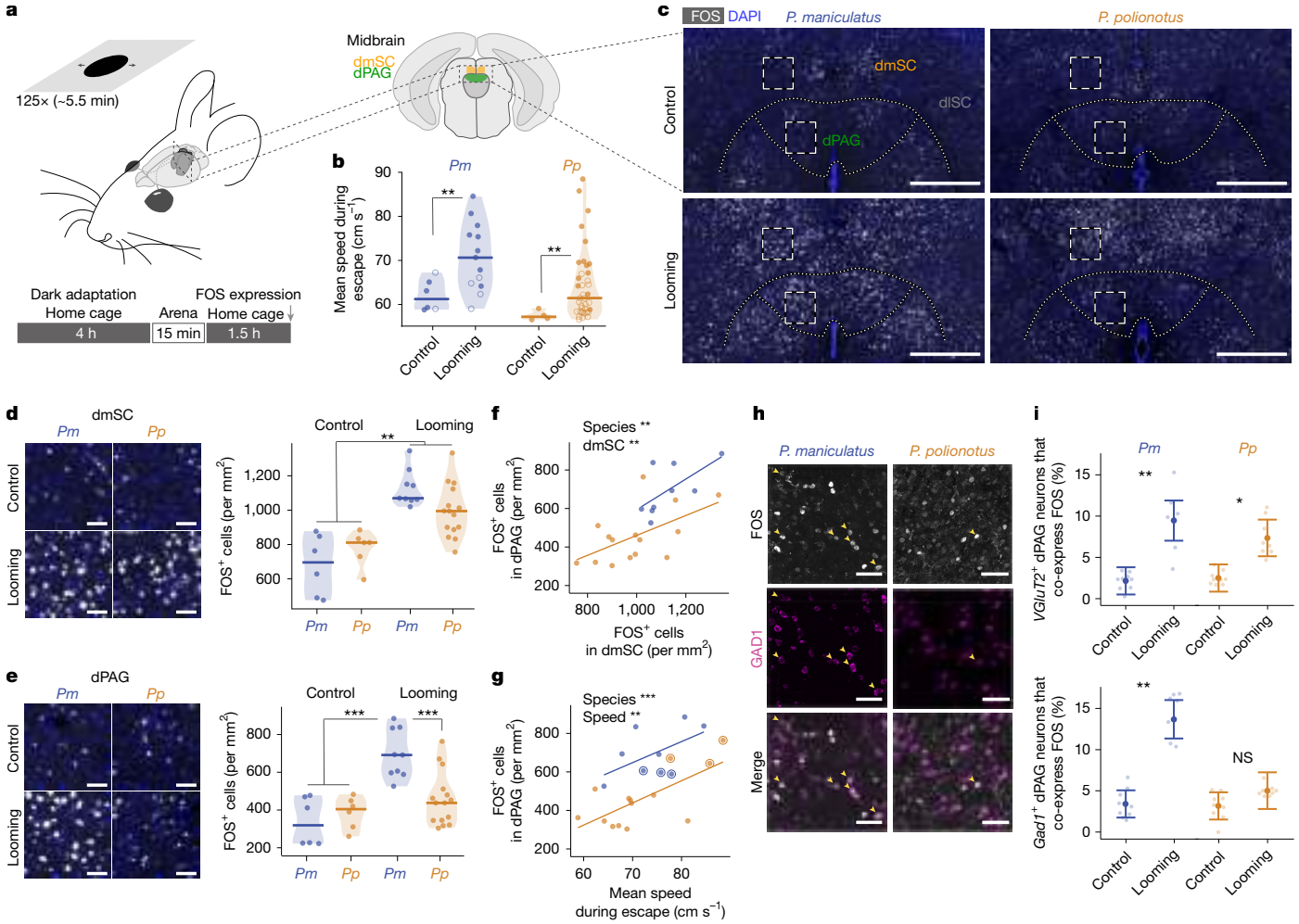

Fig. 3 | Differential activation of dPAG neurons during escape behaviour. **a**, Schematic of behavioural assay. Midbrain regions of interest: deep medial superior colliculus (dmSC) (orange) and dPAG (green). Adapted from Allen Mouse Brain Atlas (https://mouse.brain-map.org and https://atlas.brain-map.org). **b**, Mean speed during escape of *P. maniculatus* ($P = 0.001$) and *P. polionotus* ($P = 0.001$) (looming: *P. maniculatus* $n = 13$, *P. polionotus* $n = 38$; control: *P. maniculatus* $n = 6$, *P. polionotus* $n = 4$). Filled circles indicate samples stained for FOS. **c**, Representative images of FOS expression in dmSC and dPAG. Scale bars, 500 µm. Dashed white boxes indicate regions shown in **d**,**e**. dlSC, deep lateral superior colliculus. **d**,**e**, Images (left) and quantification (right) of FOS$^+$ cells in the dmSC (**d**) and dPAG (**e**) of control and looming-exposed mice (looming, *P. maniculatus*, $n = 9$; *P. polionotus*, $n = 15$; controls, $n = 6$; dSC: *P. maniculatus*, $P = 2 \times 10^{-6}$, *P. polionotus*, $P = 0.003$; dPAG: *P. maniculatus*, $P = 6 \times 10^{-6}$, *P. polionotus*, $P = 0.213$). Scale bars, 50 µm. **f**, Quantification of FOS$^+$ cells in dPAG as a function of number of FOS$^+$ cells in dmSC of looming-exposed mice (species, $P = 0.007$; dmSC, $P = 0.004$). **g**, Number of FOS$^+$ cells in dPAG as a function of mean speed during escape in looming-exposed mice (species, $P = 3 \times 10^{-4}$; speed, $P = 0.001$). Encircled points indicate samples selected for analysis in **h**,**i**. **h**, Representative images of FOS (top), GAD1 (middle) and merged (bottom) staining in the dPAG. Yellow arrowheads indicate double-labelled cells. Scale bars, 50 µm. **i**, Proportion of FOS$^+$ excitatory (*VGluT2* (also known as *Slc17a6*); top) and inhibitory (*Gad1*; bottom) dPAG neurons in subset of control and strongly escaping mice. Model fit and 95% confidence interval are shown. Points represent tissue sections (*VGluT2*, looming: *P. maniculatus* $n = 6$, *P. polionotus* $n = 8$, controls: $n = 9$; *Gad1*, looming: *P. maniculatus* $n = 7$, *P. polionotus* $n = 8$, controls: $n = 9$), collected from three mice per species (*VGluT2*, *P. maniculatus*, $P = 0.003$, *P. polionotus*, $P = 0.014$; *Gad1*, *P. maniculatus*, $P = 0.001$, *P. polionotus*, $P = 0.228$). Statistical significance evaluated with mixed-effects models.

24 escaped and 5 out of 24 froze), whereas *P. polionotus* primarily displayed freezing behaviour (1 out of 19 escaped and 15 out of 19 froze) (Fig. 2f and Supplementary Videos 6 and 7). Collectively, these data suggest that the species-specific behaviour is consistent with context- and modality-independent differences in escape threshold.

Differential dPAG activation during escape

We next sought to identify the neural circuit components that generate the observed differences in defensive behaviour. Our electrophysiological recordings in head-fixed mice suggest that visual threat information is faithfully relayed to the retinorecipient sSC in both species (Extended Data Fig. 2f–h). Moreover, we found that an aversive auditory stimulus can recapitulate the visually triggered behaviour, suggesting the neural mechanism is likely to be located downstream of visual and auditory inputs (Fig. 2f). Because the medial dSC and dPAG have a central role in mediating escape behaviours in response to both visual and auditory stimuli in rodents[27,29,35–40], we hypothesized that differences in the recruitment of these brain regions could explain the species-specific responses at the behavioural level.

To test this hypothesis, we characterized neural activation in the dSC and dPAG during an escape response, using the immediate early gene product FOS as a proxy[41]. We first confirmed that prolonged exposure to high-contrast looming stimuli triggered repeated escape in both species (as in Fig. 2). After dark adaptation, we exposed individuals to 25 sets of 5 looming stimuli, or grey background, and recorded their behavioural responses (Fig. 3a). As expected, *P. maniculatus* escaped more frequently and faster than *P. polionotus*, but escaping mice

(with more and faster escapes than control mice) could be identified in both species (Fig. 3b and Extended Data Fig. 3a,b). In a subset of these mice, representing the species-typical responses, we counted the number of FOS^+ cells (Fig. 3c). First, in looming-exposed individuals of both species, we found a larger number of FOS^+ cells, compared with control mice, in the medial dSC, but not the lateral dSC, which view the upper and lower visual field, respectively[42], consistent with the overhead position of the looming stimulus (Fig. 3d and Extended Data Fig. 3c–f). In the medial dSC, the number of FOS^+ cells correlated well with mean speed during escape but not species identity (Extended Data Fig. 3k). Thus, the dSC was active in looming-exposed mice, but levels of neural activation did not differ between species.

By contrast, the dPAG showed species-specific differences in neural activation. Overall, the number of FOS^+ cells was high in looming-exposed *P. maniculatus*, but low in *P. polionotus* (Fig. 3e and Extended Data Fig. 3g–j). Variation in dPAG activation across looming-exposed mice correlated with dSC activation and mean speed during escape, but not with the number of escapes (Fig. 3f,g and Extended Data Fig. 3l; see also Extended Data Fig. 4d,e). However, dPAG activation in *P. maniculatus* was consistently around 1.5-fold higher compared with *P. polionotus* across dSC activation levels or escape speeds (Fig. 3f,g). Thus, exposure to visual threat and resulting escape movement does not increase the number of FOS^+ cells in the dPAG of *P. polionotus* to the same extent as in *P. maniculatus*.

In *Mus*, escape is initiated by excitatory neurons in the dPAG, and its ongoing execution and termination has been linked to inhibitory dPAG neurons[27,29,43]. Using single-molecule fluorescent in situ hybridization, we examined the transmitter identity of neurons in a subset of these mice, with strong escape responses and similar numbers of FOS^+ cells in the dPAG (Fig. 3g). We found that both species possess similar numbers of excitatory and inhibitory neurons in the dSC and dPAG, and both classes are activated in the dSC of the same mice during visually evoked escape (Extended Data Fig. 3m–o). However, whereas excitatory dPAG neurons were activated in both species, we detected a higher number of FOS^+ inhibitory neurons in the dPAG of looming-exposed *P. maniculatus*, but not *P. polionotus* (Fig. 3h,i). In addition, although excitatory neurons of the dPAG were similarly activated in both species relative to dPAG neurons in general, inhibitory neurons in looming-exposed *P. maniculatus* were approximately 1.5-fold more frequently activated than expected (Extended Data Fig. 3p). Together, these immunohistochemistry results suggest that visually evoked escape in *P. polionotus* does not recruit the full ensemble of dPAG neurons, in particular inhibitory neurons, that is activated in *P. maniculatus*.

dPAG neurons encode different properties

To determine whether the differences in FOS activation during visually evoked escape arise from differences in sensory or behavioural encoding properties, we conducted Neuropixels recordings from the midbrain of each species (Extended Data Fig. 4 and Supplementary Video 8). These recordings were performed in an immersive arena, where exposure to overhead looming stimuli regularly elicited escape behaviour on a spherical treadmill (Fig. 4a–c and Methods, 'Recording immersive set-up' and 'Visual stimuli immersive set-up'). To quantify the preference of each neuron for escape movements over visual stimuli alone, we first calculated a behavioural selectivity index by comparing the correlation of neural activity with looming diameter while mice were stationary to the correlation of neural activity—after subtracting the average visual response—with running speed during visually evoked escapes (Extended Data Fig. 5a,b; adapted from ref. 44). We observed a similar preference for looming stimuli across neurons in the sSC and dSC of both species. By contrast, the behavioural selectivity of dPAG neurons was greater in *P. maniculatus* than in *P. polionotus* during escape epochs (Fig. 4d,e). Consistent with this, we further found that putative escape neurons in the dPAG of *P. maniculatus* had weak and delayed visual responses, similar to the dPAG of *Mus* where escape neurons show unreliable visual responses[27,43] (Fig. 4f). By contrast, in *P. polionotus*, strong visual responses were observed across the sSC, dSC and dPAG, and putative escape neurons had similar visual responses to other neurons (Fig. 4f and Extended Data Fig. 5d). We found similar species differences in analyses of maximum firing rate, and with analyses based on linear regression (Fig. 4g,h and Extended Data Fig. 5e–h). These findings link neural activity in the dPAG of *P. maniculatus* to the behavioural execution of escape, and suggest that the increased FOS^+ levels in the dPAG of *P. maniculatus* (Fig. 3) arise from species-specific escape-related neural activity. In *P. polionotus*, dPAG activity instead appears to originate largely from peri-escape exposure to visual stimuli (Extended Data Fig. 5r–t).

To further disentangle and characterize stimulus and behaviour-related activity, we recorded from midbrain neurons while mice either viewed visual stimuli on a computer monitor or spontaneously escaped (Methods, 'Recording monitor set-up' and 'Visual stimuli monitor set-up'). Neurons in both *P. maniculatus* and *P. polionotus* displayed similar visual responses, with a strong preference for looming over dimming stimuli, and similar response dynamics to looming stimuli of different expansion speeds (Extended Data Fig. 6a–f). Similar to visually evoked escapes, however, we found the neural activity of the dPAG in *P. maniculatus*, but not in *P. polionotus*, to closely follow the running speed during spontaneous escapes (Fig. 4i and Extended Data Fig. 6g–i).

Together, these immunohistochemistry and electrophysiology experiments indicate that visual threat can trigger neural activity in the superior colliculus and dPAG of both species. However, whereas dPAG neurons encode escape events in *P. maniculatus*, dPAG activity does not correlate with the initiation of running behaviour in *P. polionotus*, suggesting the dPAG may contain the neural circuits on which evolution has acted.

Functional manipulation of dPAG neurons

To investigate the causal role of the dPAG in mediating behaviours, we optogenetically activated neurons in the dPAG of both *P. maniculatus* and *P. polionotus*. We injected an adeno-associated virus (AAV2) vector bilaterally into the dPAG to express channelrhodopsin, or only the YFP reporter for controls, in predominantly excitatory neurons, under the control of the CamKII promoter (Fig. 5a and Extended Data Figs. 7–9). Using a centrally implanted optic fibre (Fig. 5b), we stimulated the dPAG as mice moved freely in a circular arena. The trajectory and speed of each mouse was extracted, and each trial was classified as acceleration, deceleration or 'other' on the basis of the behaviour of the mouse during the stimulation (Fig. 5c–e, Extended Data Fig. 8e–g, Supplementary Videos 9–13 and Methods). We found that the proportion of acceleration and deceleration trials differed between the species (Fig. 5f,g and Extended Data Fig. 8h,i). Specifically, *P. polionotus* displayed more deceleration trials (Fig. 5h), and *P. maniculatus* displayed more acceleration trials (Fig. 5i) during optogenetic stimulation, compared with controls. These species differences in evoked behaviours were robust across different types of behaviour parameterization (Extended Data Fig. 9). Consistent with FOS^+ cell numbers (Fig. 3), increasing laser power during optogenetic stimulation triggered more and faster acceleration events in *P. maniculatus*, whereas the speed of both acceleration and deceleration events decreased in *P. polionotus* (Fig. 5i–k and Extended Data Fig. 8h–j). Similar species differences in acceleration could be triggered when mice were still (Extended Data Fig. 8k–m). These results suggest that activation of dPAG neurons has opposing effects in the two species: *P. maniculatus* tend to accelerate, whereas *P. polionotus* predominantly decelerate.

To explore the extent to which dPAG neurons are required for the species-specific behaviours, we next expressed inhibitory DREADDs receptors (hM4d(Gi)-mCherry), or only the mCherry reporter for controls, in the dPAG. Three weeks later, we injected either the ligand CNO

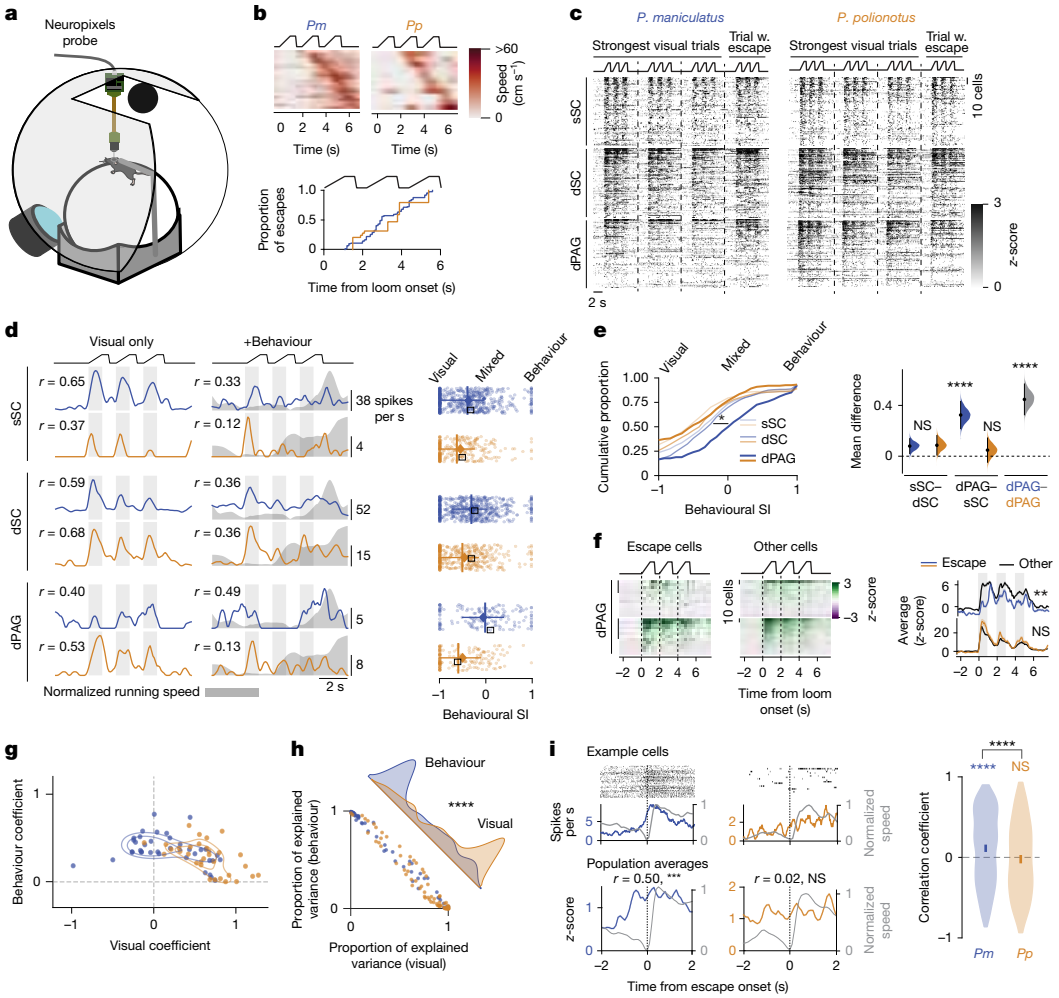

Fig. 4 | Species-specific encoding of locomotion in the dPAG. a, Schematic of immersive set-up. **b**, Running speed (top) and escape onset (bottom) during triple loom stimuli. *P. maniculatus*, $n = 6$ mice; *P. polionotus*, $n = 4$. **c**, Concatenated responses of 100 cells per area for trials with highest stimulus correlation (column 1–3) and one escape trial (last column). **d**, Example cells in the sSC, dSC and dPAG during stimuli without (left) and with (middle) escape, and corresponding Spearman coefficients. Right, behavioural selectivity index (SI) for each neuron. Vertical lines indicate median, horizontal lines represent interquartile range and diamonds show the mean. Squares indicate example cells. **e**, Cumulative distributions (left; dPAG–dPAG $P = 3 \times 10^{-10}$; *P. maniculatus* sSC–dPAG $P = 0.012$, dSC–dPAG $P = 0.021$) and quantification (right; sSC–dSC *P. maniculatus* $P = 0.554$, *P. polionotus* $P = 0.162$; *P. polionotus* dPAG–sSC $P = 0.072$) of data from **d**. **f**, Responses of putative escape cells (left) and other cells (middle) in the absence of escape. Mean ± s.e.m. of heatmaps (blue/gold: putative escape cells; black: other cells) (right). Statistics compare mean response during first loom ($P = 0.006$, $P = 0.667$). **g**, Linear regression weights of all cells with a positive behaviour coefficient. Contours: 20–40%. **h**, Relative explained variance (separate r^2/combined r^2). Density along diagonal represents difference of proportion of explained variance (visual − behaviour). $P = 3 \times 10^{-5}$. **i**, Example neurons (top) and population averages (bottom) for trials with escape response >2 × s.d. (monitor set-up) (*P. maniculatus*, $n = 217$ trials, 3 mice; *P. polionotus*, $n = 194$, 3 mice). Data are mean activity ± s.e.m. (blue or gold) and mean speed ± s.e.m. (grey). Distributions of correlations of peri-escape activity (right). Vertical lines: 95% confidence intervals, *P. maniculatus* $P = 1 \times 10^{-12}$, *P. polionotus* $P = 0.561$, between species $P = 7 \times 10^{-16}$. Two-sided, two-sample Kolmogorov–Smirnov test (**e**, left, **h**), two-sided unpaired mean difference Gardner–Altman estimation (**e**, right, **i**), two-sided Brunner–Munzel test (**f**).

or saline and exposed the mice to five repetitions of a 100% contrast looming stimulus (Fig. 5l). As expected from previous experiments (Fig. 2b), saline-injected *P. maniculatus* escaped earlier and with greater vigour than *P. polionotus* (Fig. 5m,n, Extended Data Fig. 8n and Supplementary Videos 14–17). By contrast, CNO-injected *P. maniculatus* delayed the onset of escape, such that the cumulative proportion of escape in CNO-injected *P. maniculatus* was no longer distinguishable from that in *P. polionotus*. Notably, inhibition of dPAG neurons had little effect on the cumulative proportion of freezing behaviour, suggesting that the dPAG facilitates freezing in *P. polionotus* (Fig. 5g,h) but is not the main driver of this behaviour (Fig. 5n and Extended Data Fig. 6j–r). Together, these results suggest that inhibition of dPAG neurons increases the escape threshold in *P. maniculatus*, but does not affect the ability of either species to escape.

Collectively, our findings, together with the FOS analysis and in vivo electrophysiological recordings, demonstrate that the dPAG in *P. maniculatus* specifically mediates rapid, low-threshold escape, but that it does not have the same functional role and thereby increases the threshold to escape, in *P. polionotus*.

Discussion

Here we show that ecologically distinct, yet closely related, species of deer mice evolved a species-specific difference in defensive behaviour. Specifically, when exposed to a looming stimulus, *P. polionotus* requires a higher threat intensity to reliably trigger escape relative to both *P. maniculatus* and *P. leucopus*. We trace this behavioural difference to a central brain region, the dPAG, which we show no longer encodes

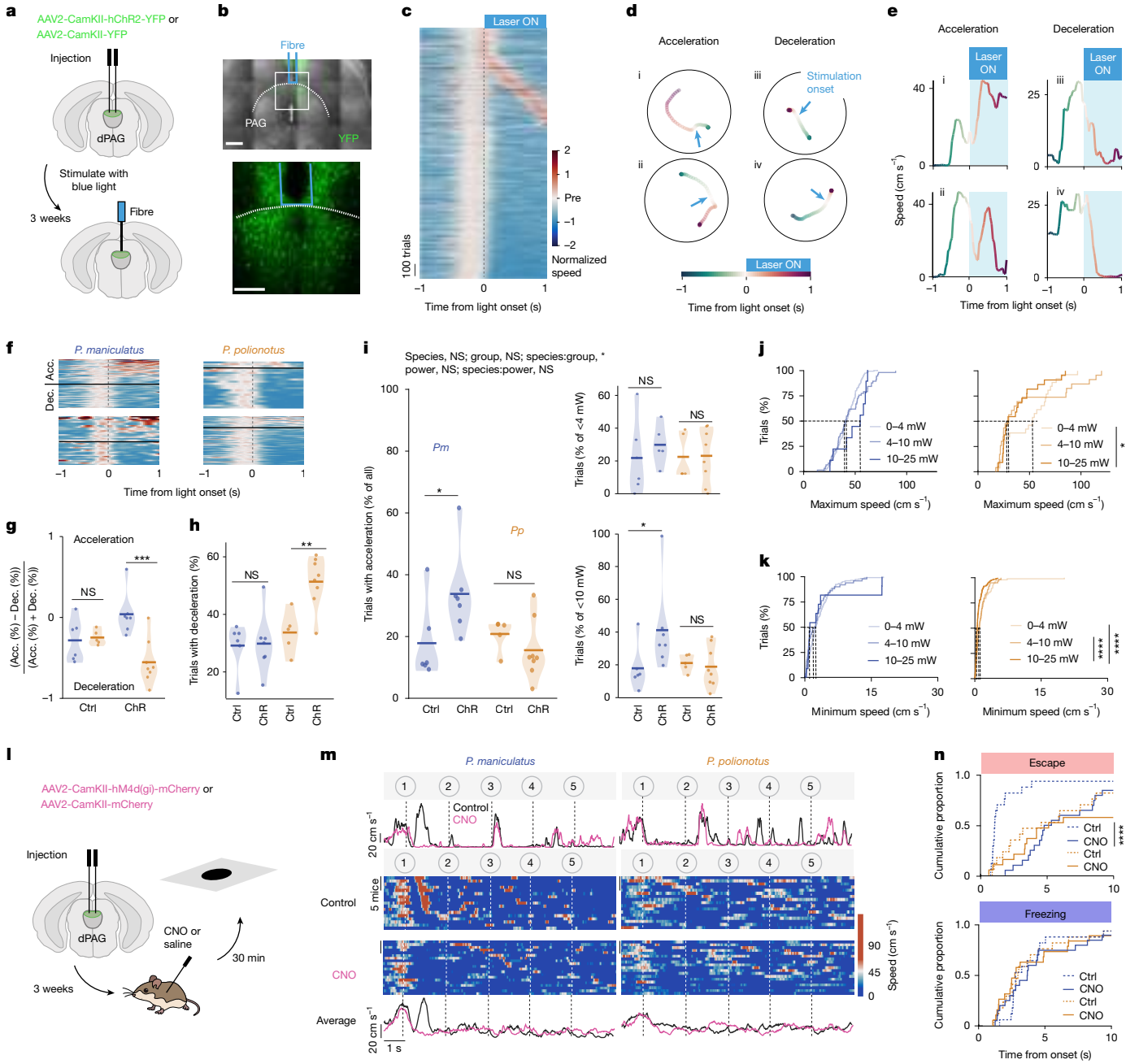

Fig. 5 | Activation and inhibition of dPAG neurons recapitulates species differences. a, Experimental paradigm for optogenetic activation of the dPAG. Mice were injected with hChR2-containing or hChR2-free (control) constructs. **b**, YFP-ChR2$^+$ neurons (green) and optic fibre tract (blue) in the dPAG. Scale bar: 400 µm (top), 200 µm (bottom). **c**, Normalized speed (to 0.37 s before laser ON) from all trials, sorted by extrema. **d**, Example trajectories illustrating acceleration (i, ii; see Supplementary Videos 9 and 10) and deceleration (iii, iv; see Supplementary Videos 11 and 12). **e**, Speed traces for trajectories in **d**. **f**, Traces from four mice 1 s before and during laser stimulation. **g**, Percentage difference between acceleration and deceleration trials for each mouse. Horizontal lines indicate the mean (*P. maniculatus*: ChR $n = 7$, sham $n = 6$; *P. polionotus*: ChR $n = 8$, sham $n = 5$). Sham: $P = 0.788$, ChR: $P = 0.0004$. Ctrl, control. **h**, Percentage of deceleration trials per mouse. $P = 0.933$, $P = 0.006$. **i**, Percentage of acceleration trials. All trials (left; $P = 0.048$, $P = 0.307$), <4 mW laser power (top right; $P = 0.485$, $P = 0.956$) and <10 mW (bottom right; $P = 0.045$, $P = 0.731$). ANOVA species: group $P = 0.010$, group $P = 0.052$, species $P = 0.053$, other $P > 0.6$. **j**, Maximum speed during acceleration trials for each laser power range. **k**, Minimum speed during deceleration trials. **l**, Experimental paradigm for chemogenetic inhibition of the dPAG. Mice were injected with hM4d(Gi)-containing or hM4d(Gi)-free (control) constructs. **m**, Example speed traces during looming stimuli after saline (control) or CNO injection (top) (see Supplementary Videos 14–17). Speed traces for control (hM4d(Gi) + saline or mCherry + CNO) and all CNO (hM4d(Gi) + CNO) trials (centre). Average speed traces (bottom). **n**, Cumulative distributions of escape and freezing events. Two-sided unpaired mean difference Gardner–Altman estimation (sham versus ChR; **g**–**i**), two-sided, two-sample Kolmogorov–Smirnov test (**j**,**k**,**n**), two-way ANOVA (**i**). Brain schematics adapted from Allen Mouse Brain Atlas (https://mouse.brain-map.org and https://atlas.brain-map.org).

and initiates escape-related movements in *P. polionotus* to the same extent as in *P. maniculatus*.

It is possible that the observed species-specific behaviour evolved via natural selection. In dense fields or forests, escape (for example, darting to a refuge) may increase survival probability, whereas in open environments movement is often conspicuous and freezing could minimize predator detection. However, when exposed to an intense threat (such as imminent attack), escape may be the only option for

survival. This explanation is consistent with the observation that *Mus* are more likely to freeze in the absence of a refuge[33], and more broadly with the distinct strategies observed in other species to avoid predator detection in different environments[45–47].

Our behavioural and neural recording experiments suggest that the neural basis for these ecologically relevant behavioural differences is located centrally in the brain. First, both visual and auditory stimuli evoked similar species-specific behavioural responses. Second, visual looming stimuli trigger similar patterns of neural activity across the entire depth of the superior colliculus. Together, these data indicate that the key neural mechanism lies downstream of both the retina and the confluence of sensory inputs in the dSC. Indeed, our neural recording and manipulation experiments identify the dPAG, a subregion of the PAG implicated in driving escape behaviour[32], as a likely locus that differentiates the two species. Specifically, rapid escape and running movements correlated well with activity in the dPAG of *P. maniculatus* but not *P. polionotus* (Figs. 3 and 4). Moreover, activation of dPAG neurons triggered running and acceleration in *P. maniculatus*, but deceleration and stopping in *P. polionotus*. Further, inhibition of the dPAG eliminated early and vigorous escape responses to visual looms in *P. maniculatus*, making their responses appear identical to those of *P. polionotus* (Fig. 5). These findings highlight the role of a central brain structure in species-specific behaviour, different from many studies that link behavioural evolution to peripheral sensory systems[48–51], and demonstrate that differences in how neurons in the dPAG of *P. maniculatus* and *P. polionotus* process behavioural information are key to understanding the species-specific behaviours.

Our data are consistent with a model in which the threshold to escape is controlled differently in the brains of *P. maniculatus* and *P. polionotus*. In mice, multiple inhibitory pathways, both within the dPAG/lateral PAG and projecting from other brain areas, have been shown to modulate the excitability of putative escape neurons in the dPAG[43,52–56]. We propose that one or multiple of these modulatory inputs has evolved to attenuate the excitability of escape neurons in *P. polionotus*. This model is consistent with our finding that both species possess comparable proportions of excitatory and inhibitory neurons in the dPAG (Fig. 3), and that neurons in the dPAG of *P. maniculatus* and *P. polionotus* exhibit similar levels of intrinsic excitability (Extended Data Fig. 10).

In addition, as both species appeared to retain the ability for late-onset escape during inhibition of the dPAG, partially redundant, dPAG-independent escape pathways are likely to exist. Whereas the dorsal division of the PAG primarily controls escape behaviours[57,58], neurons that mediate escape and freezing behaviours are intermingled in both the dorsal and lateral divisions of the PAG[58]. In addition, circuits that bypass the PAG—for example, via the parabigeminal or cuneiform nuclei—can also initiate escape[20,39,59,60]. By attenuating the relative contribution of the dPAG-dependent pathway to the computation of escape decisions, evolution may have capitalized on this parallel circuit architecture to raise the escape threshold in *P. polionotus*, suggesting that circuit architecture can facilitate evolutionary change in behaviour.

Future work is aimed at determining the cellular and molecular mechanisms that explain why incoming threat information does not recruit to the same extent the ensemble of excitatory and inhibitory dPAG neurons in *P. polionotus*, unlike *P. maniculatus*, for the execution of escape. Although our findings highlight the dPAG as the most upstream node that has evolved species-specific properties, they do not exclude further changes downstream of the dPAG.

Here we show that ecologically distinct deer mice evolved species-specific defensive behaviours and trace this difference to a central brain region, the dPAG. Together our data suggest that evolution can adjust a behaviour dial by shifting the threshold between two conserved behaviours—freezing and escape—to fine-tune defensive response in different environments, providing a rare example of a central brain region linked to natural variation in a sensory-driven behaviour.

Online content

Any methods, additional references, Nature Portfolio reporting summaries, source data, extended data, supplementary information, acknowledgements, peer review information; details of author contributions and competing interests; and statements of data and code availability are available at https://doi.org/10.1038/s41586-025-09241-2.

1. McBride, C. S. et al. Evolution of mosquito preference for humans linked to an odorant receptor. *Nature* **515**, 222–227 (2014).
2. Auer, T. O. et al. Olfactory receptor and circuit evolution promote host specialization. *Nature* **579**, 402–408 (2020).
3. Baldwin, M. W. et al. Evolution of sweet taste perception in hummingbirds by transformation of the ancestral umami receptor. *Science* **345**, 929–933 (2014).
4. Wada-Katsumata, A., Silverman, J. & Schal, C. Changes in taste neurons support the emergence of an adaptive behavior in cockroaches. *Science* **340**, 972–975 (2013).
5. Bedford, N. L. & Hoekstra, H. E. *Peromyscus* mice as a model for studying natural variation. *eLife* **4**, e06813 (2015).
6. Tierney, A. J. Evolutionary implications of neural circuit structure and function. *Behav. Proc.* **35**, 173–182 (1995).
7. Cande, J., Prud'homme, B. & Gompel, N. Smells like evolution: the role of chemoreceptor evolution in behavioral change. *Curr. Opin. Neurobiol.* **23**, 152–158 (2013).
8. Seeholzer, L. F., Seppo, M., Stern, D. L. & Ruta, V. Evolution of a central neural circuit underlies *Drosophila* mate preferences. *Nature* **559**, 564–569 (2018).
9. Roberts, R. J. V., Pop, S. & Prieto-Godino, L. L. Evolution of central neural circuits: state of the art and perspectives. *Nat. Rev. Neurosci.* **23**, 725–743 (2022).
10. Tinbergen, N. Social releasers and the experimental method required for their study. *Wilson Bull.* **60**, 6–51 (1948).
11. Tinbergen, N. *The Study of Instinct* (Clarendon Press/Oxford University Press, 1951).
12. Ball, W. & Tronick, E. Infant responses to impending collision: optical and real. *Science* **171**, 818–820 (1971).
13. De Franceschi, G., Vivattanasarn, T., Saleem, A. B. & Solomon, S. G. Vision guides selection of freeze or flight defense strategies in mice. *Curr. Biol.* **26**, 2150–2154 (2016).
14. Hatsopoulos, N., Gabbiani, F. & Laurent, G. Elementary computation of object approach by a wide-field visual neuron. *Science* **270**, 1000–1003 (1995).
15. Holmqvist, M. H. A visually elicited escape response in the fly that does not use the giant fiber pathway. *Vis. Neurosci.* **11**, 1149–1161 (1994).
16. Schiff, W., Caviness, J. A. & Gibson, J. J. Persistent fear responses in rhesus monkeys to the optical stimulus of "looming". *Science* **136**, 982–983 (1962).
17. Temizer, I., Donovan, J. C., Baier, H. & Semmelhack, J. L. A visual pathway for looming-evoked escape in larval zebrafish. *Curr. Biol.* **25**, 1823–1834 (2015).
18. Yamamoto, K., Nakata, M. & Nakagawa, H. Input and output characteristics of collision avoidance behavior in the frog *Rana catesbeiana*. *Brain Behav. Evol.* **62**, 201–211 (2003).
19. Yilmaz, M. & Meister, M. Rapid innate defensive responses of mice to looming visual stimuli. *Curr. Biol.* **23**, 2011–2015 (2013).
20. Westby, G. W. M., Keay, K. A., Redgrave, P., Dean, P. & Bannister, M. Output pathways from the rat superior colliculus mediating approach and avoidance have different sensory properties. *Exp. Brain Res.* **81**, 626–638 (1990).
21. Basso, M. A. & May, P. J. Circuits for action and cognition: A view from the superior colliculus. *Annu. Rev. Vis. Sci.* **3**, 197–226 (2017).
22. Wheatcroft, T., Saleem, A. B. & Solomon, S. G. Functional organisation of the mouse superior colliculus. *Front. Neural Circuits* **16**, 792959 (2022).
23. Gale, S. D. & Murphy, G. J. Distinct representation and distribution of visual information by specific cell types in mouse superficial superior colliculus. *J. Neurosci.* **34**, 13458–13471 (2014).
24. Gale, S. D. & Murphy, G. J. Distinct cell types in the superficial superior colliculus project to the dorsal lateral geniculate and lateral posterior thalamic nuclei. *J. Neurophysiol.* **120**, 1286–1292 (2018).
25. May, P. J. The mammalian superior colliculus: laminar structure and connections. *Prog. Brain Res.* **151**, 321–378 (2006).
26. Xie, Z. et al. Transcriptomic encoding of sensorimotor transformation in the midbrain. *eLife* **10**, e69825 (2021).
27. Evans, D. A. et al. A synaptic threshold mechanism for computing escape decisions. *Nature* **558**, 590–594 (2018).
28. Lefler, Y., Campagner, D. & Branco, T. The role of the periaqueductal gray in escape behavior. *Curr. Opin. Neurobiol.* **60**, 115–121 (2020).
29. Deng, H., Xiao, X. & Wang, Z. Periaqueductal gray neuronal activities underlie different aspects of defensive behaviors. *J. Neurosci.* **36**, 7580–7588 (2016).
30. Tsang, E. et al. Induction of flight via midbrain projections to the cuneiform nucleus. *PLoS ONE* **18**, e0281464 (2023).
31. Abrams, P. A. The evolution of predator-prey interactions: Theory and evidence. *Annu. Rev. Ecol. Syst.* **31**, 79–105 (2000).
32. Branco, T. & Redgrave, P. The neural basis of escape behavior in vertebrates. *Annu. Rev. Neurosci.* **43**, 417–439 (2020).
33. Vale, R., Evans, D. A. & Branco, T. Rapid spatial learning controls instinctive defensive behavior in mice. *Curr. Biol.* **27**, 1342–1349 (2017).
34. Mongeau, R., Miller, G. A., Chiang, E. & Anderson, D. J. Neural correlates of competing fear behaviors evoked by an innately aversive stimulus. *J. Neurosci.* **23**, 3855–3868 (2003).
35. Bittencourt, A. S., Nakamura-Palacios, E. M., Mauad, H., Tufik, S. & Schenberg, L. C. Organization of electrically and chemically evoked defensive behaviors within the deeper collicular layers as compared to the periaqueductal gray matter of the rat. *Neuroscience* **133**, 873–892 (2005).

36. Coimbra, N. C., Leão-Borges, P. C. & Brandão, M. L. GABAergic fibers from substantia nigra pars reticulata modulate escape behavior induced by midbrain central gray stimulation. *Braz. J. Med. Biol. Res.* **22**, 111–114 (1989).
37. Vargas, L. C., de Azevedo Marques, T. & Schenberg, L. C. Micturition and defensive behaviors are controlled by distinct neural networks within the dorsal periaqueductal gray and deep gray layer of the superior colliculus of the rat. *Neurosci. Lett.* **280**, 45–48 (2000).
38. Wei, P. et al. Processing of visually evoked innate fear by a non-canonical thalamic pathway. *Nat. Commun.* **6**, 6756 (2015).
39. Shang, C. et al. A parvalbumin-positive excitatory visual pathway to trigger fear responses in mice. *Science* **348**, 1472–1477 (2015).
40. Sahibzada, N., Dean, P. & Redgrave, P. Movements resembling orientation or avoidance elicited by electrical stimulation of the superior colliculus in rats. *J. Neurosci.* **6**, 723–733 (1986).
41. Bullitt, E. Expression of C-fos-like protein as a marker for neuronal activity following noxious stimulation in the rat. *J. Comp. Neurol.* **296**, 517–530 (1990).
42. Dräger, U. C. & Hubel, D. H. Responses to visual stimulation and relationship between visual, auditory, and somatosensory inputs in mouse superior colliculus. *J. Neurophysiol.* **38**, 690–713 (1975).
43. Stempel, A. V. et al. Tonically active GABAergic neurons in the dorsal periaqueductal gray control instinctive escape in mice. *Curr. Biol.* **34**, 3031–3039.e7 (2024).
44. Chen, X. et al. Brain-wide organization of neuronal activity and convergent sensorimotor transformations in larval zebrafish. *Neuron* **100**, 876–890.e875 (2018).
45. Wheatley, R., Pavlic, T. P., Levy, O. & Wilson, R. S. Habitat features and performance interact to determine the outcomes of terrestrial predator–prey pursuits. *J. Anim. Ecol.* **89**, 2958–2971 (2020).
46. Lima, S. L. & Dill, L. M. Behavioral decisions made under the risk of predation: a review and prospectus. *Can. J. Zool.* **68**, 619–640 (1990).
47. Wywialowski, A. P. Habitat structure and predators: choices and consequences for rodent habitat specialists and generalists. *Oecologia* **72**, 39–45 (1987).
48. Seehausen, O. et al. Speciation through sensory drive in cichlid fish. *Nature* **455**, 620–626 (2008).
49. Lloyd, E. et al. Blind cavefish retain functional connectivity in the tectum despite loss of retinal input. *Curr. Biol.* **32**, 3720–3730 (2022).
50. Montgomery, S. H., Rossi, M., McMillan, W. O. & Merrill, R. M. Neural divergence and hybrid disruption between ecologically isolated *Heliconius* butterflies. *Proc. Natl Acad. Sci. USA* **118**, e2015102118 (2021).
51. Rossi, M. et al. Adaptive introgression of a visual preference gene. *Science* **383**, 1368–1373 (2024).
52. Tovote, P. et al. Midbrain circuits for defensive behaviour. *Nature* **534**, 206–212 (2016).
53. Fadok, J. P. et al. A competitive inhibitory circuit for selection of active and passive fear responses. *Nature* **542**, 96–100 (2017).
54. Fratzl, A. et al. Flexible inhibitory control of visually evoked defensive behavior by the ventral lateral geniculate nucleus. *Neuron* **109**, 3810–3822.e3819 (2021).
55. Salay, L. D. & Huberman, A. D. Divergent outputs of the ventral lateral geniculate nucleus mediate visually evoked defensive behaviors. *Cell Rep.* **37**, 109792 (2021).
56. Li, C. et al. Pathway-specific inputs to the superior colliculus support flexible responses to visual threat. *Sci. Adv.* **9**, eade3874 (2023).
57. Fanselow, M. S. Neural organization of the defensive behavior system responsible for fear. *Psychon. Bull. Rev.* **1**, 429–438 (1994).
58. Stempel, A. V. A conserved brainstem region for instinctive behaviour control: the vertebrate periaqueductal gray. *Curr. Opin. Neurobiol.* **86**, 102878 (2024).
59. Shang, C. et al. Divergent midbrain circuits orchestrate escape and freezing responses to looming stimuli in mice. *Nat. Commun.* **9**, 1232 (2018).
60. Mitchell, I. J., Dean, P. & Redgrave, P. The projection from superior colliculus to cuneiform area in the rat. *Exp. Brain Res.* **72**, 626–639 (1988).

Publisher's note Springer Nature remains neutral with regard to jurisdictional claims in published maps and institutional affiliations.

Open Access This article is licensed under a Creative Commons Attribution-NonCommercial-NoDerivatives 4.0 International License, which permits any non-commercial use, sharing, distribution and reproduction in any medium or format, as long as you give appropriate credit to the original author(s) and the source, provide a link to the Creative Commons licence, and indicate if you modified the licensed material. You do not have permission under this licence to share adapted material derived from this article or parts of it. The images or other third party material in this article are included in the article's Creative Commons licence, unless indicated otherwise in a credit line to the material. If material is not included in the article's Creative Commons licence and your intended use is not permitted by statutory regulation or exceeds the permitted use, you will need to obtain permission directly from the copyright holder. To view a copy of this licence, visit http://creativecommons.org/licenses/by-nc-nd/4.0/.

© The Author(s) 2025

Methods

Mouse strains and husbandry

Colony founders of *P. maniculatus bairdii* (strain BW), *P. polionotus subgriseus* (strain PO) and *P. leucopus* (strain LL) were originally obtained from the *Peromyscus* Genetic Stock Center at the University of South Carolina and then established and maintained at Harvard University. *M. musculus* (C57BL/6 J strain) were purchased from The Jackson Laboratory. Behaviour, FOS and RNAscope experiments were performed at Harvard and, later, optogenetics, chemogenetics and in vivo recording experiments were performed at Neuro-Electronics Research Flanders (NERF).

Housing at Harvard University: mice were housed on Bed-o'Cobs 1/4-inch bedding (The Andersons) in ventilated standard rodent cages (Allentown) on a 16 h light: 8 h dark cycle at 23 °C with ~20–30% humidity. We provided mice with a red translucent polycarbonate hut, Enviro-Dri nesting material, and a cotton nestlet. All mice were given ad libitum access to irradiated Prolab Isopro RMH 3000 5P74 (LabDiet) and water.

Housing at NERF: mice were housed on Lignocel 3–4 bedding (J. Rettenmaier & Söhne) in ventilated standard rodent cages on a 12 h light:12 h dark cycle at 23 °C with 50% humidity (40–60%). Mice were provided with cotton nesting material. All mice were given ad libitum access to chow diet (ssniff) and water.

After weaning litters at 23 days of age, we kept same sex mice in groups of up to 5 individuals by strain, unless otherwise indicated. Mice of either sex were between two and six months old at the time of experiments.

All experiments were performed as approved by the Institutional Animal Care and Use Committee (IACUC) of Harvard University, and Animal Ethics Committee of KU Leuven.

Animal usage

In total, data were collected from 14 *M. musculus* and 633 *Peromyscus* (including *P. maniculatus*, *P. polionotus* and *P. leucopus*) across a series of behavioural, electrophysiological, molecular and optogenetic experiments. For behavioural assays with a sweep–looming stimulus, we tested 14 *M. musculus* (two trials per mouse), 30 *P. maniculatus*, 29 *P. polionotus* and 36 *P. leucopus* (1 trial per mouse). Repeated looming stimuli with varying contrast were presented to 109 *P. maniculatus* and 116 *P. polionotus* (two trials each), while single looming and auditory stimuli, as well as control conditions (for example, hut removal, 2× expansion speed, dimming), were tested in additional cohorts (19–30 mice per group, one trial per mouse). For FOS mapping, repeated looming was used in 21 *P. maniculatus* and 66 *P. polionotus*. AAV expression was verified using single-molecule fluorescence in situ hybridization (smFISH) in three mice per species. Neuropixels recordings during evoked behaviour (immersive set-up) were conducted in 6 *P. maniculatus* and 4 *P. polionotus*, with 10 and 5 total recordings, respectively; spontaneous activity was recorded in 4 *P. maniculatus* and 3 *P. polionotus* using a monitor-based set-up. Optogenetic activation experiments using ChR2 were performed in 7 *P. maniculatus* and 8 *P. polionotus*, with controls (no opsin expression) tested in 6 and 5 mice, respectively. Chemogenetic inhibition using hM4D(Gi) and CNO was tested in 13 mice per species; additional groups received saline then CNO ($n = 9$) or mCherry then CNO ($n = 5$) per species. Contrast response curves were measured in one mouse per species to complement the main cohorts. Finally, in vitro electrophysiological recordings were conducted in 11 *P. maniculatus* and 10 *P. polionotus*. Inclusion and exclusion criteria are described in the corresponding sections below. Unless mentioned there, all trials from all mice were included in the analysis.

Behaviour experiments

Experimental set-up. To assay behavioural response to a visual stimulus, we constructed a rectangular behavioural arena from plexiglass that measured 45 cm (W) × 30 cm (D) × 30 cm (H), adapted from ref. 19. We attached a triangular prism-shaped hut (24 cm (W) × 18 cm (D) × 12 cm (H)) to one corner of arena floor. To reduce reflection, we covered the arena walls and floor with Matte Finish (Krylon). To illuminate the arena, we lined the outside base of the walls with infrared light (IR) LED strips. To record behaviour from below the arena, we made the ground floor of IR-transmissive black plexiglass and used an IR-sensitive camera (Flea3 FL3-FW, monochrome, Point Grey Research) to record at 30 fps. We programmed visual stimuli with Psychtoolbox-3 for Matlab[61,62] and displayed them on an LCD monitor from above the arena. Finally, we triggered an LED (invisible to the mouse) simultaneous to the visual stimulus through an Arduino Uno connected to the computer, which we used to synchronize individual frames with the stimulus. We generated sound stimuli with a power amplifier (TB10A, Fosi Audio) connected to a tweeter (Pro-TW120, DS18).

Experimental procedure. Before each behavioural experiment, mice were left undisturbed in their cage for 24 h. We conducted all experiments within the first 4 h of the dark period (Zeitgeber time) and in red light. We habituated mice to the experiment room for 30 min, and then transferred a single individual to the behavioural arena, where it habituated for 10 min. We triggered the stimulus manually when the mouse moved away from the walls towards the centre of the arena and recorded the behaviour of the mouse for 2–3 min before and after the stimulus was triggered. Once testing was complete, we moved the individual to an empty cage and wiped out the arena with 70% ethanol. We then assayed the remaining individuals in the cage following the same protocol.

For the contrast experiment, we randomly assigned a new cohort of mice and exposed each mouse once to a contrast level. Approximately 1 week (range of 5–11 days) after the first exposure, we again randomly assigned the same individuals to a different contrast level and exposed them once. We employed this approach to both minimize habituation from repeated testing and to reduce the number of mice needed for the experiment. For all other experiments (sweep–looming, looming with hut, looming without hut, dimming, auditory), we used new cohorts of naive mice and exposed individuals to the stimulus only once.

To determine which brain region(s) show activity correlated with behavioural response, we collected the brains of mice following their exposure to the overhead stimulus. To this end, we single-housed mice in a new cage the day before the experiment. On the test day, we dark habituated the mice by moving their cage in the test room for 4 h. We then gently transferred mice to the arena, with the hut closed off. After 10 min of habituation, we triggered the stimulus. We recorded the behaviour of mice during the complete trial. We then transferred mice back into the cage and transcardially perfused them after 90 min in the dark (see below).

Stimuli. To quantify response to a visual stimulus, we first conducted an assay with a combined sweep–looming stimulus[13]. The stimulus was a black disc on grey background with a diameter of ~4° visual angle (approximately 2.2 cm) that first appeared in one corner of the computer screen and slowly moved diagonally at a speed of 10° s^{-1}. Once the disc reached the centre of the screen, it rapidly expanded to a diameter of 40° visual angle (approximately 22 cm) at a linear speed of 36° s^{-1}. The disc then remained at full diameter for 2 s before disappearing. We chose these parameters because preliminary experiments revealed that they maximized the difference in behavioural response between the two focal species. For example, a linear expansion speed of 72° s^{-1} reduced the species-specific responses (Extended Data Fig. 1g).

To measure the behavioural response of mice to different levels of threat, we altered the contrast of the looming disc by changing its intensity against the standard grey background. Intensity is indicated as a positive percentage, converted from the negative Weber fraction[27]. We used different contrast levels of the looming disc: 32%, 55%, 72%, 86%

and 100%, with one additional contrast level for each species within its dynamic range (*P. maniculatus*: 45%; *P. polionotus*: 97%). Contrast values were validated with a digital illuminance meter (LX1330B, Dr. Meter). The stimulus comprised 5 repeats of the standard looming stimulus, with a remain time at full diameter of 0.5 s and an inter-stimulus period of 0.5 s (ref. 27).

To test the behavioural response to an aversive auditory stimulus, we exposed mice in the looming arena to an ultrasound frequency upsweep (17–20 kHZ over 1.3 s, repeated 5 times; 80 dB at arena floor), while the visual screen displayed a grey background[33,34].

To test the effect of a refuge on behavioural response, we exposed mice to a single looming stimulus (black disc on grey background) in the presence of the hut. As before, the stimulus remained at full diameter for 2 s before disappearing. To test the effect of the absence of a refuge, we closed off the hut and exposed mice to the same single looming stimulus.

To test the behavioural response to a non-moving, innocuous visual stimulus, we used a disc of fixed size (diameter of 40°) that appeared in the centre of the screen, initially matching the grey background but then changing to black over 1 s and remaining black for 2 s before disappearing.

To quantify FOS levels after defensive behaviour, we exposed mice to 125 repeats of the standard looming stimulus, structured into 25 sets of 5 repeats, with a remain time at full diameter of 0.5 s, an inter-stimulus period of 0.5 s within sets, and an inter-set period of 3 s. Control mice were exposed to only the standard grey background.

Analysis. To characterize the behavioural response of an mouse to the stimulus, we used a custom Matlab (v.2015b or newer) code to retrieve centroid coordinates of the mouse and the status of the stimulus from the video recordings. We calculated the speed of each mouse from these coordinates and smoothed the data using a mean filter with a width of five frames.

'Escaping' is typically defined as running at speeds above a data-derived threshold and towards a refuge, while the definition of 'freezing' varies across studies, but often refers to the absence of movement defined by very low displacement thresholds[13,19,55,63]. Here, we classified behaviours based on data-derived thresholds, but without additional constraints on movement direction. Specifically, we automatically annotated escape events as a speed $\geq$55.74 cm s^{-1}, and freezing events as a continuous period of $\leq$3.28 cm s^{-1} for at least 0.4 s while the mouse was outside the hut (see Extended Data Fig. 1). We arrived at these definitions by comparing behaviour during exposure to a single looming stimulus to baseline behaviour. For this experiment, we analysed a video segment for each mouse with a duration of 1 s that preceded stimulus exposure by 1–2 min. We selected these video segments such that they matched our criterion for triggering a stimulus (see above; that is, when the mouse moved away from the walls towards the centre of the arena). We recorded escape speed as the maximum speed during the escape event.

For the sweep–looming experiment, trials in which the mouse was in the hut at the onset of the looming stimulus were removed (*P. maniculatus*, $n = 1$; *P. polionotus*, $n = 3$; *P. leucopus*, $n = 8$); we compared only mice that were exposed to the full stimulus.

In the contrast looming experiment, we assumed that mice had definitively detected the stimulus if two independent observers unanimously confirmed a discernible response (that is, interruption or commencement of body movement) during the first looming repeat (Extended Data Fig. 2c,d).

To test for the effect of the presence or absence of a hut, we removed mice that did not show evidence of detecting the stimulus (hut present: *P. maniculatus*, $n = 1$; *P. polionotus*, $n = 1$; hut absent: *P. maniculatus*, $n = 0$; *P. polionotus*, $n = 2$).

FOS immunohistochemistry

Immunohistochemistry and imaging. To measure neuronal activity of mice exposed to a looming stimulus, we used the immediate early gene product FOS as a marker of neuronal activity. Following the behaviour experiment described above, we transcardially perfused mice with ice-cold 1× phosphate-buffered saline and then with 4% paraformaldehyde. Brains were dissected out, postfixed for 24 h at 4 °C, cryopreserved in 30% sucrose, and stored at −70 °C until subsequent use. We selected a subset of these mice that represented the species-typical distribution in escape number and speed (Fig. 3b and Extended Data Fig. 3a,b) for FOS immunohistochemistry. To stain for FOS protein, we sectioned brains at 40 µm, blocked tissue for 1 h, and incubated sections for 2 days with rabbit anti-FOS antibody (1:4,000, Synaptic Systems, 226003). We used donkey anti-rabbit Alexa 647 antibody (1:1,000, Invitrogen, A31573) for secondary detection and mounted tissues with DAPI Fluoromount-G (SouthernBiotech, 0100-20). Slides were imaged on an AxioScan.Z1 slide scanner (Zeiss).

Analysis. Following imaging, we exported images to.tif format and arranged sections into anterior–posterior order with the ImageJ plugin TrakEM2[64]. We manually outlined regions of interest (ROIs) with custom Fiji (v.2.1.0 or more recent)[65] macros based on landmark structures identified using autofluorescence patterns and DAPI staining. For the dPAG, we included the medial and lateral subdivisions (dm/dlPAG). To segment images, we used the ImageJ plugin StarDist[66] with default parameters (model – versatile, normalize image – yes, percentile low – 1, percentile high – 99.8, probability – 0.5, overlap threshold – 0.4), which automatically detects cells using neural network models with star-convex shape priors. For each identified cell in the dataset, we retrieved the area, *xy* coordinates, and mean intensity. We filtered out large artefacts that were incorrectly identified as cells by removing objects with an area of >180 μm^2. Across the ROIs (superior colliculus and PAG) in each section, we then counted cells with mean intensities larger than the mode of the density function of mean intensities as FOS-positive. With this approach, we filtered out cells with the lowest FOS expression, to enrich for cells that were activated during the behavioural experiment, and to remove any batch effects (for example, baseline FOS expression levels across experiments).

Single-molecule fluorescence in situ hybridization

Experimental procedure. To determine whether FOS^+ cells were excitatory or inhibitory neurons, we selected, from our previous FOS experiment, three individuals of each species with strong escape responses and high levels of FOS^+ cells, as well as three control mice for combined smFISH and immunohistochemistry processing. We obtained six sections (thickness 14 µm) from each mouse, and then used half to detect *NeuN* (also known as *Rbox3*), *Gad1* and FOS, and the other half to detect *NeuN*, *VGluT2* and FOS. Seven out of the 72 sections did not have reliable staining and were excluded from the dataset. To determine if $AAV2^+$ cells were primarily excitatory or inhibitory, we injected three mice of either species with the viral vector (see 'Virus injection and fibre implantation') and then obtained 6 sections (thickness 14 µm) from each mouse and used half to detect *Gad1* and YFP, and the other half to detect *VGluT2* and YFP.

smFISH protocol. We used the RNAscope Multiplex Fluorescent Reagent Kit v2 with the RNA-Protein Co-Detection Ancillary Kit for co-detection of mRNA and protein. For smFISH, we used custom-made RNAscope probes for *Gad1*, *VGluT2* and *NeuN*. Probes were based on the coding sequence of each gene, and single-nucleotide polymorphisms were included by alternating between species (*P. maniculatus* and *P. polionotus*). For immunohistochemistry, we used rabbit anti-FOS (1:100, Synaptic Systems, 226003) and rabbit anti-GFP (1:100, Thermo Fisher, A-11122) to detect FOS protein and the YFP tag in the viral vector, respectively, and horseradish peroxidase-labelled goat anti-rabbit antibody (1:500, PerkinElmer, NEF812001EA) for secondary detection. We visualized RNA probes and antibodies with Opal 520, Opal 570, and Opal 690 dyes (1:1000, Akoya Biosciences, FP1487001KT, FP1488001KT,

FP1497001KT), and counterstained with DAPI. ROIs (mSC, dPAG) were imaged on a LSM 700 laser scanning confocal microscope (Zeiss), with *z*-stacks of 21 slices spaced at 0.99 µm. We then used QuPath v0.2.3 to quantify the overlap of FISH and immunohistochemistry signals in the maximum projection images.

Analysis. For the FOS–RNAscope experiment, we assigned neuron and transmitter identity to cells by defining section-specific cutoffs as the mode of the density function of the log-transformed distribution of RNA punctae number minus half (for *NeuN*) or one time (for *VGluT2* and *Gad1*) the standard deviation of the distribution of RNA punctae number. We defined cells as neurons or as excitatory or inhibitory when they had at least three *NeuN* or *VGluT2*/*Gad1* punctae, respectively, and exceeded the section-specific cutoffs. From this dataset, we then calculated the following three variables: percentage of neurons that co-express a given transmitter, percentage of transmitter-positive neurons that co-express FOS, and enrichment ratio (percentage of transmitter-positive neurons that co-express FOS, divided by percentage of neurons that co-express FOS). For the complete dataset, we then generated a mixed-effects linear model [response ~ (variable + species + stimulus + transmitter + brain region)^5 + section ID] using the R package lme {lme4}, and evaluated the model by contrasting stimulus (percentage of transmitter-positive neurons that co-express FOS) or species (percentage of neurons that co-express a given transmitter, enrichment ratio) with emmeans {emmeans} and contrast {emmeans}. We adjusted *P* values with the Benjamini–Hochberg method.

In vivo Neuropixels probe recordings

Headpost surgery. Mice of each species (2–4 months old) were anaesthetized with isoflurane (Iso-vet; 3% for induction, 1–3% during surgery), placed into a stereotaxic system (Narishige, SR-5N), and dura tear (Novartis, 288/28062–7) was applied to protect their eyes. After removing the hair on the head with depilation creme, we injected lidocaine (Xylocaine 0.5%, 0.007 mg g^{-1}) under the skin above the skull and then incised the scalp along the midline to reveal the skull. A metal headpost was fixed on the skull using dental cement (Superbond C&B, Prestige-dental). The mice received a single injection of buprenorphine (0.2 mg kg^{-1} intraperitoneal injection) and antibiotics (Emdotrim; 1 ml per 100 ml) in the drinking water for the next 3–5 days.

Experimental procedure. After at least 3 days of recovery, the mice were anaesthetized briefly and a craniotomy above the superior colliculus was performed using a dental drill. Still under anaesthesia, we transported the mice to the recording set-up. For recordings of the same mouse on later days, we briefly anaesthetized the mouse in its cage and transported it to the recording set-up. Mice were fixed with their headpost on a ball floating on air (polystyrene white ball, 20 cm diameter). Two recording set-ups were used (see 'Recording monitor set-up' and 'Recording immersive set-up').

A Neuropixels probe version 1.0 or phase 3A[67] (imec) coated with a fluorescent dye (DiD, DiI or DIO; Thermofisher) was lowered slowly into the right superior colliculus and dPAG. We targeted the centre of the superior colliculus based on anterior–posterior coordinates and the portion next to the midline to detect responses to the upper visual field. We then covered the exposed brain and skull with artificial cerebrospinal fluid (150 mM NaCl, 5 mM potassium, 10 mM D-glucose, 2 mM NaH_2PO_4, 2.5 mM $CaCl_2$, 1 mM $MgCl_2$, 10 mM HEPES adjusted to pH 7.4 with NaOH).

This set-up allowed mice to walk and run on the ball, with tight control over their field of view. Twenty minutes after insertion of the probe, we started the presentation of visual stimuli. Following the recordings, the mice were euthanized, and the probe location was verified by confocal images of the fluorescent dye in 200-µm-thick slices stained with DAPI. We included recordings only in cases in which the probe went through the sSC and dSC as well as the dPAG, and in which we could detect clear light responses in the superior colliculus.

Recording monitor set-up. This set-up was used to characterize visual response properties and to analyse spontaneous escape behaviour. We presented visual stimuli on a 32-inch LCD monitor (Samsung S32E590C, 1,920 × 1,080 pixel resolution, 60 Hz refresh rate, average luminance of 2.6 cd m^{-2}) with the lower part of the monitor placed 35 cm in front of the left eye of the mouse (covering 90° of azimuth and 70° of altitude) and at an angle so that the distance between the eye of the mouse to the left corner, right corner and top of the monitor was comparable. A Neuropixels probe was lowered slowly into the brain and after reaching the target depth, we waited for 20 min for the neural activity to stabilize and for the mouse to settle on the ball. Although head-fixed, due to the possibility to move 'freely' on the ball, mice did not require further habituation to the set-up. Once settled, we presented visual stimuli and recorded the neural activity with the Neuropixels probe and the movement of the mouse on the ball with two motion sensors (Tindie, PMW3360). We recorded the 384 electrodes (16 µm lateral spacing, 20 µm vertical spacing) at the tip of the probe, covering 3,840 µm in depth. Signals were recorded at 30 kHz using the Neuropixels headstage (imec), base station (imec), and a Kintex-7 KC705 FPGA (Xilinx). High frequencies (>300 Hz) and low frequencies (<300 Hz) were acquired separately. To select the recording electrodes, adjust gain corrections, observe online recordings, and save data, we used SpikeGLX V20230101-phase30 software (https://billkarsh.github.io/SpikeGLX). We simultaneously recorded the timing of visual stimulation using digital ports of the base station.

Visual stimuli monitor set-up. Visual stimuli were presented on a grey background and were controlled by Octave (GNU Octave) and Psychtoolbox (http://psychtoolbox.org)[61,68]. Here, we analysed visual responses to 10 repetitions of a black looming disk (from 4° to 50° visual angle in 0.3 s; the disk stayed at full size for 0.5 s before a 3 s grey background) and a dimming disk that stayed at a size of 50° visual angle and changed from grey to black within 0.3 s. All mice were tested under dim daylight conditions (normal screen brightness or 1 log unit darker). For some mice, we conducted additional recordings under moonlight conditions (3–4 log units darker). We used all light conditions to test for a correlation between running speed and neural activity; however, we used only daylight conditions for visual response analysis. To measure contrast response curves, we displayed looming discs of different contrasts in a randomized order with randomized inter-stimulus times of 3–7 s, resulting in 8–12 repetitions of each contrast (5, 15, 25, 35, 45, 60, 75, 90 and 97% Weber contrast).

Recording immersive set-up. This set-up was used to analyse looming-evoked escape. Recordings on the immersive display were performed as in 'Recording monitor set-up', with the following differences. Mice were fixed with their headpost in the centre of a panoramic display (50 cm diameter) as described above. Visual stimuli were presented with a projector (DLPDLCR3010EVM-G2 (TI), 1,280 × 720 pixel resolution, 60 Hz refresh rate, average luminance of 5 cd m^{-2}) projecting through a condenser (Canon EF 50 mm F1.4 USM) and a fisheye lens (Peleng 8 mm f3.5 Fisheye Lens M42). The timing of visual stimulation was detected with a photodiode on the fisheye lens. Signals were recorded at 30 kHz using the Neuropixels headstage (imec, HS_1000) connected to a Neuropixels PXIe acquisition module (imec, PXIE_1000) in a PXIe chassis (NI, PXIe 1071). Stimulation timing from the photodiode and ball data acquisition timing were recorded by a PXIe I/O Module (PXIe-6341, sampling rate = 30,488 Hz) in the PXIe chassis. The ball data was recorded using Bonsai V2.6.2 (https://bonsai-rx.org/). An Arduino sent a synchronization signal to both the I/O and Neuropixels modules simultaneously, allowing the alignment of data recorded on the I/O module and the Neuropixels acquisition module.

Visual stimuli immersive set-up. We presented visual stimuli using a custom-made visual stimulation software (OpenGL-based).

We presented 20 repetitions of a black looming stimulus on a grey background (97% Weber contrast). Each looming stimulus consists of three presentations of a black disk expanding from 4° to 40° visual angle in 1 s, the black disk remaining at full size for 0.5 s, followed by 0.5 s background (triple loom stimulus). Each set of 3 consecutive looms is separated by a $\log_{10}$ random time interval between 10 s and 3.5 min ($(((\log_{10}(r \times 9.9 + 0.1) + 1)/2) \times 200 + 10)$, with r drawn from a uniform distribution in the interval [0,1]. The stimuli were presented at 55° elevation. At the beginning of each experiment, we additionally presented a 4° sweeping white square to estimate the receptive field location of the recorded neurons. The white square was presented at each azimuth ranging from 0° to 80° with 15° intervals on the right side of the mouse. For subsequent stimuli, we selected the azimuth that evoked the strongest response to the sweeping white square.

Spike sorting. We sorted the high-pass filtered neural data using Kilosort2[69] (https://github.com/MouseLand/Kilosort/releases/tag/v2.0), followed by manual curation in phy2 (https://github.com/cortex-lab/phy). Units were labelled as a real unit based on their waveform shape and auto-correlogram. We used cross-correlograms to identify spikes in different units that belong to the same cell. For subsequent analysis, we used only single unit data. We identified borders between the sSC and dSC as well as the dSC and dPAG using histological sections, spiking activity, and in some cases, clustering of raw spiking activity, similar to ref. 70 (Extended Data Fig. 4). The probe tract was extracted from the tracer labelling together with the known insertion depth. The upper borders of the sSC and dPAG could be clearly identified in the histological sections and the relative electrode numbers were extracted. The border between the sSC and dSC was extracted from the raw spiking activity during looming stimuli and based on previous measurements of sSC thickness using labelling of retinal axons with choleratoxin B (data not shown). Finally, the lower border of the dPAG was based on a conservative estimate from the histological sections, like for the FOS analysis. The placement of the probe close to the midline (that is, upper visual field) minimized the inclusion of lateral PAG neurons.

Contrast response curves. To calculate contrast response curves, we used looming responses of neurons in the sSC. First, we calculated firing rates during each contrast in 100 ms bins and then subtracted background activity before stimulus onset. Then, we averaged firing rates at each contrast and normalized the data by setting peak firing rates at no stimulation (0% contrast) to 0 and the maximum firing rate at any other contrast to 1. We identified responding neurons as cells with: (1) at least 10 significant responses (more than 3× s.d. of mean pre-stimulus activity) at any contrast (out of 90 total stimulations); (2) detectable responses to the highest presented contrasts; and (3) no sudden response drop at intermediate contrasts.

Looming selectivity index. We calculated preferences for looming or dimming stimuli from full-contrast stimuli. We calculated firing rates as the number of spikes in 20 ms bins and extracted average peak firing rate (P_l for looming and P_d for dimming) during multiple repetitions of the stimuli. We defined the looming selectivity index (LSI) as: $LSI = (P_l - P_d)/(P_l + P_d)$.

Locomotion events. In head-fixed mice, escape and freezing bouts were qualitatively similar to freely moving escaping and freezing, i.e. sudden onsets of running bouts or sudden immobility for a short time period. However, there are some differences to the freely moving setting: head-fixed mice tend to move less between stimuli and do not reach the same running speeds. We hence used relative rather than absolute criteria that capture these similarities (sudden onset, large enough change from pre-stimulus behaviour) for extraction of escape and freezing bouts. Specifically, to extract evoked and spontaneous escape and freezing periods, we binned the measured running speed to achieve the same temporal resolution as the neural activity (100-ms bins) and normalized it such that 'no movement' is set to 0 and maximum acceleration speed set to 1. Then, we identified time points of onset of escape and freezing. We defined the onset of escape as: an acceleration of >0.2 a.u. within 200 ms after a speed of <0.05 a.u. We defined freezing as: a deceleration (negative speed difference of >0.1 a.u.) from a speed of >0.1 a.u. to a speed of <0.05 a.u. For analysis of spontaneous locomotion, we included only events that were not preceded by a visual stimulus onset in the previous 1 s.

Neural activity during locomotion. We calculated the z-score of neural activity of sorted single units. For data from the monitor set-up, i.e. spontaneous escape events, the z-score was calculated as the firing rate binned in 100 ms bins minus the mean firing rate during seconds −3 to −1 before escape/freezing onset, and divided by the standard deviation across the entire recording. For data from the immersive set-up, i.e. looming-evoked escape events, the mean firing rate and standard deviation was calculated during the 2.5 s before the first looming onset.

Evoked escape analysis. We presented 20 repetitions of a triple loom stimulus (see 'Visual stimuli immersive set-up') in an immersive arena to examine how individual neurons encode visual looming stimuli and escape events. Escape responses occurred in a subset of trials. Below we describe three calculations based on this dataset: (1) behavioural selectivity index (BSI); (2) analysis of escape neurons; and (3) linear regression analysis.

Behavioural selectivity index. We calculated two BSIs, one based on correlations and the second based on peak firing rate. For each, estimates of visual responsiveness were based on trials that did not include an escape, and estimates of behaviourally related activity on trials that included a visually triggered escape. To estimate visually related neural activity, we calculated the Spearman correlation between the z-scored neural activity (from non-escape trials) and the disk diameter of the stimulus (scaled from 0 (no disk) to 1 (maximum disk size)). The correlation was calculated over a 10 s window, spanning 2.5 s before stimulus onset to 1.5 s after the final loom. For each neuron, we defined its visual response (C_v) as the average of the three highest Spearman correlation coefficients observed across all trials. Representative examples of single-cell responses for these top three trials are shown in Fig. 4c. To estimate behaviourally related neural activity, we analysed trials in which escape behaviour occurred. We first computed a visual template as the average neural activity of all trials without behaviour and subsequently subtracted this template from each escape trial to obtain the residual neural activity. We then calculated the Spearman correlation between this residual activity and running speed from 2 s before to 2 s after escape onset. The average of these correlation coefficients is the behavioural correlation (C_b). Example single-cell activity during looming trials with an escape event is shown in Fig. 4c (right column). The BSI was then calculated as: $BSI = (C_b - C_v)/(C_b + C_v)$. The data for this version of BSI are shown in Fig. 4d,e.

To evaluate the robustness of our findings, we repeated this analysis using maximum firing rates instead of correlation coefficients. First, we extracted the maximum firing rates during the first loom (FR_v) and during escape events (FR_b). A behavioural selectivity index based on firing rate (BSIFR) was then calculated as: $BSIFR = (FR_b - FR_v)/(FR_b + FR_v)$. The data for this version of BSI are shown in Extended Data Fig. 5e.

Analysis of escape neurons. Putative escape neurons were identified using either correlations or peak firing rates. To identify putative escape neurons using correlations, we compared the behavioural correlation (C_b; as defined above) to a random correlation (C_n) based on a shuffled set of trials. Specifically, C_n was computed as the Spearman

correlation between speed traces from escape trials and neural activity during non-escape trials. Neurons were classified as putative escape neurons if they met the criteria $C_b > 0$ and $C_b > C_n$. The data are shown in Extended Data Fig. 5c.

To identify putative escape neurons using peak firing rates, we compared each neuron's peak firing rate to the average response of all neurons. In Mus studies, escape neurons exhibit weak or no visual responses[43]. Therefore, putative escape neurons were identified as those with a $FR_b >$ threshold (9 spikes per s) and $FR_v <$ threshold (9 spikes per s). This threshold is the average peak response during escapes of all trials and mice. Results are presented in Extended Data Fig. 5f, with the peri-escape firing rate analysis shown in Extended Data Fig. 5l,p,t.

To evaluate similarities in visual responses between putative escape neurons and other cells, we computed each neuron's mean response during the first loom presentation. The distributions of these mean responses during the first loom were compared using the Brunner–Munzel test (Fig. 4f).

Linear regression analysis. To assess the relationship between visual and behavioural responses, we fit a linear regression model to predict spike counts from speed and stimulus traces, based on the top three visual trials and all trials where escape behaviour occurred. Neural activity was binned into 500 ms intervals, and the mean spike count per bin was calculated. Notably, different bin sizes (1 s, 1.5 s, or 2 s) did not change the results (all $P < 0.0001$). Stimulus traces were binarized (0, absence; 1, presence of the visual stimulus) and speed traces and spike counts were standardized using *z*-scores.

Statistics. Spearman correlations were computed using the corr function in MATLAB and Julia (v.1.11). The two-sample Kolmogorov–Smirnov test was calculated using kstest2 in MATLAB. Effect sizes and confidence intervals were estimated using DABEST. This included bootstrap-based estimations using 5,000 resampled datasets to compute unpaired mean differences (Gardner–Altman estimation). *P* values were adjusted for multiple comparisons and represent the likelihood of observing the effect size under the null hypothesis. The regression model was implemented using LinearRegression().fit from the scikit-learn package in Python (v.3.6.0 or newer). Model fits were evaluated using explained variance, R^2. Cells with $R^2 > 0.1$ were included in further analysis. To determine the relative contributions of speed vs. visual stimulus, we computed R^2 ratios: R^2_speed_ratio = R^2_speed_only/R^2_full, and R^2_stim_ratio = R^2_stim_only/R^2_full.

Spontaneous locomotion–activity correlation. To correlate spontaneous movement events and the corresponding neural activity, we calculated the mean neural activity during each event (−2 to +2 s from onset of escape or freezing). We then calculated the correlation coefficient of the speed trace and the average neural activity using 'corr' in Matlab across the full 4 s. Only trials with a *z*-score > 2 during the event were included in Fig. 4. Results did not change for a threshold of 4 and analyses using that threshold are included in Extended Data Fig. 6. We estimated the 95% confidence intervals per species as well as for a Gaussian distribution with mean 0 and the same variance using DABEST[71].

Optogenetic activation experiments

Virus injection and fibre implantation. To optogenetically activate dPAG neurons, we injected a viral vector into the dPAG, followed by implantation of an optic fibre. We followed the same procedure as for headpost surgery. Following the craniotomy, we injected 50–100 nl of viral vector (AAV2/CamkII-hChR2(E123T/T159C)-p2A-EYFP-WPRE, UNC vector core, AV5456B or AVV2/CamkII-EYFP for control mice) bilaterally into the dPAG (*P. maniculatus*, lambda: +0.9 mm, midline: ±0.2 mm, depth: −2.9–3.2 mm; *P. polionotus*, lambda: +0.8 mm, midline: ±0.2 mm, depth: −2.6–2.9 mm) with a micropipette (Warner Instrument, G100-4) with an open tip of 30 µm attached to a microinjector IM-9B (Narishige). In two mice (one of each species), a modified injection protocol was used in which the virus was injected into the same location but at an angle of 30°. In both cases, we lowered the micropipette to a position 0.1–0.2 mm below the targeted depth for 2 min, and then brought it up to the injection depth. After 1 min, we slowly injected the virus with a hand-wheel. After 5 min, we retracted the micropipette and closed the skin using Vetbond tissue adhesive (3M, 1469). After surgery, we provided antibiotics (Emdotrim, ecuphar, BE-V235523) via drinking water. Either during or approximately 3 weeks after the viral injection, we anaesthetized mice as described above and implanted an optic fibre (200 µm diameter, length 3.5 mm, NA 0.39, Doric Lenses, B280-2304-3.5) above the injection sites (*P. maniculatus* depth: −2.5–3.1 mm, *P. polionotus* depth: −2.4–2.6 mm). Due to the large blood vessels at the midline, we first lowered the fibre into the brain lateral adjacent to the central blood vessel and then gently pushed it towards the midline and lowered it to the target depth by alternating steps of moving 100–200 µm down and up until the target depth was reached. We affixed the fibre with dental cement (Sun Medical LTD). After surgery, we injected mice with one dose of buprenorphine (0.2 mg kg^{-1} intraperitoneal injection) and provided antibiotics (Emdotrim) in their drinking water for 3–5 days. We single-housed mice following surgery and gave them 7–20 days to recover before behavioural testing.

Experimental procedure. To test the effects of optogenetic dPAG activation on behaviour, we briefly anaesthetized mice in their home cage with isoflurane, transferred them to a round arena (diameter: 43 cm) and connected them to a patch cord with a rotatory joint (Thorlabs, RJPFL2). Mice typically woke up within 1–2 min and started exploring the arena. We illuminated the arena with dim red light and video recorded behaviour with a camera (Point Grey Research, FMVU-03MTM-CS or Basler, acA1300-60gmNIR) positioned 53 cm above the centre of the arena. We then used a DPSS laser system (Laserglow Technologies, R471003GX) or a diode laser (Laserglow Technologies, D4B2003FX) to deliver 50 Hz light pulses (10 ms on, 10 ms off) of 473 or 470 nm over 1 s through an optical fibre attached to the optic implant while the mice were freely moving in the arena. We verified laser power at the output of the patch cord without a fibre before and after recording sessions with a power meter (Thorlabs, PM100D with S130C sensor). Laser powers ranged from 0.3 to 24.1 mW.

We began experiments with low laser powers (<1 mW output at the patch cord) and increased laser power in steps of 1–5 mW to find a regime producing consistent behaviour. We then further investigated the effects of differing power levels below and above. Optogenetic triggers were sent manually using an Arduino when the mouse was moving spontaneously through or along the walls of the arena. The session was terminated when the mice stopped cooperating (that is, sat still for a prolonged time or started running erratically); most mice required more than one session to complete the measurements. We recorded videos at 30 Hz using PylonRecorder2 (Basler) or Bonsai[72]. After optogenetic experiments, mice were anaesthetized with isoflurane and decapitated.

Analysis of virus expression and fibre location. To analyse viral expression and confirm the location of the fibre, we fixed the brains of test and control mice overnight in 4% paraformaldehyde and then sliced them coronally into 200 µm thick slices with a vibratome. We washed the slices three times in PBS/0.5% Triton X-100 and then incubated them with primary chicken anti-GFP (Thermo Fisher, A-10262 1:200) to stain for YFP that was co-expressed with Chr2 or YFP for control mice overnight at 4 °C. After washing with PBS/0.5% Triton X-100, we incubated slices with the secondary antibody (Alexa 488 donkey anti-chicken, Immuno Jackson, 703-545-155, 1:500) and DAPI (Roche, 10236276001) for 2 h at room temperature. After washing with

PBS, we mounted slices on coverslips, covered them with mounting medium (Dako, C0563), and imaged them using 10× and 63× objectives on a confocal microscope.

Using this approach, we were able to exclude mice with no or little YFP staining in the dPAG or with incorrect fibre placements (inside the dPAG or >250 µm above the dPAG). For the remaining mice, we then analysed the extent and location of the Chr2 expression and the fibre placement. First, we took confocal images of the 200 µm slice where the fibre was most visible (*z*-stack, 10× objective). We then loaded raw images into Fiji[65] and identified the slice with the brightest YFP staining and with a clear fibre tract. We split the imaged channels (Chr2 and DAPI) and ran the StarDist 2D plugin[66] on the Chr2 channel (parameters: model – versatile, normalize image – yes, percentile low – 10, percentile high – 99, probability – 0.2, overlap threshold – 0.4). We measured and saved the area and *xy* position of each detected, labelled cell with an area <1,000 pixels. We loaded png versions of the maximum intensity projections into Matlab to manually label the extent of the dPAG, the fibre tip, the outline of the ventricle and a control area without detected cells. We quantified the extent of viral infection as the number of detected cells within the dPAG below the fibre tip. Further, we quantified the area of dPAG with viral expression as percentage of the dPAG area with an intensity value above the mean +2× s.d. control area intensity. We analysed the relationship between YFP expression, fibre location, and running behaviour by calculating the correlation (corr in Matlab) between percentage running trials with number of YFP cells, distance between fibre and dPAG surface, and percentage of dPAG area with labelling.

Analysis of optogenetically induced behaviour. We extracted the head position of mice from each video with DeepLabCut[73] (v.2.1.9 or newer) and used this to estimate the movement speed of each mouse during optogenetic stimulation. We excluded trials (that is, laser triggers) for which the mouse moved less than 10 cm s^{-1} on average during the 0.5 s before the laser trigger.

Optogenetic experiments are fundamentally different from the freely moving and head-fixed experiments for two reasons: first, it creates an artificial, highly synchronized activation of a population of neurons that likely is not exactly the same as the activation triggered by a looming stimulus. Second, for practical reasons (that is, the requirement for a light-weight and hence short optic fibre cable), optogenetic experiments were performed in a small arena, limiting the possibilities for speed and behaviour kinetics. To clarify this difference, we used the terms acceleration and deceleration to describe the behaviour observed in this experiment. Acceleration was defined by a forward acceleration during the 1 s period of optogenetic stimulation, as determined by observing both a sharp increase in speed during the stimulus and visual inspection to ensure the movement was forward. Deceleration was defined as a continuous time period (>400 ms) with speeds below 70% of the baseline speed, confirmed by visual inspection. All remaining trials were classified as "other". We used these classifications to calculate the percentage of acceleration and deceleration trials (Fig. 5g–i).

In addition, we computed a speed index (SI) and adjusted speed index (adjSI) to compare the speed during the main behaviour with a baseline as follows: $\text{adjSI} = (\text{Speed}_{\text{Behaviour}} - \text{Speed}_{\text{Baseline}})/(\text{Speed}_{\text{Behaviour}} + \text{Speed}_{\text{Baseline}})$. For the SI, the 'baseline' was calculated as the mean speed in the 0.37 s before laser onset and the 'behaviour' was defined as the mean speed during the laser trigger. For the adjusted SI, the main behaviour (behaviour) was centred around the maximum for forward movement trials and minimum for slowing trials. The baseline period (baseline) was defined as the 0.37 s (11 frames) before the behaviour event. In either case, this computation resulted in positive values for acceleration and negative values for trials in which the mouse decelerated. A final parameter used to compare the sham and experimental groups consisted of the steepest slope during the laser trigger. Again, the slope parameter was positive for acceleration and negative for deceleration trials.

To compare triggered and sham mice as well as different laser powers, we performed three statistical tests: an ANOVA test, a two-sample Kolmogorov–Smirnov test (kstest2 in MATLAB) and estimation of effects size and confidence intervals using DABEST[71]. For the latter, for effect size estimation, unpaired mean difference Gardner–Altman estimation was performed, in which 5,000 bootstrap samples were taken and the mean difference between two groups was calculated together with the confidence interval. The *P* value reported is the likelihood of observing the effect size if the null hypothesis of no difference is true.

Chemogenetic inhibition experiments

Virus injection. To chemogenetically inactivate dPAG neurons, we injected 50–100 nl of viral vector (AAV2/CamkIIa-hM4D(GI)-mCherry, Addgene 50477- AAV2 or AVV2/CamkIIa-mCherry, Addgene 114469 – AAV2, for control mice) bilaterally into the dPAG. The procedure was the same as in previous surgeries (head-posting, optogenetic experiments). Mice were tested at least five weeks after the viral injection.

Experimental set-up. To assess the effect of chemogenetic manipulation on visually guided behaviour, we used a custom arena (80 cm (L) × 34 cm (D) × 50 cm (H)) with a red-tinted transparent acrylic floor and a display monitor (LG 34UM69G-B, 34 inch diagonal class 21:9, 250 cd m^{-2} mean luminance, 60 Hz refresh rate) positioned above the arena. Light levels in the arena were kept dim (>10 lux) by adding a logarithmic filter on the screen. In the arena, we included a shelter, with a triangular prism-shape (H: 10 cm, L: 24 cm, W: 11 cm), made from the same material as the platform, and positioned in one corner of the arena. Below the floor, the arena was lined with infrared LED strips. We recorded the behaviour of the mouse from below the arena with a near-IR camera (Basler, acA1300-60g mNIR, 60 fps) with a fixed 6 mm focal lens (Ricoh Lens, FL-CC0614A-2M). Visual stimuli were presented with BonVision V0.11.0[74]. The synchronization of the camera and the presentation of the stimuli were controlled using customized Bonsai workflows.

Experimental procedure. Before each experiment, we briefly anaesthetized mice with isoflurane (<30 s) and intraperitoneally injected CNO (1 mg kg^{-1}) or saline (same corresponding volume). Following the injection, mice were single-housed in a new cage and transferred into the behavioural room to habituate for 30 min. For acclimatization to the arena, mice were allowed to freely explore it for 10 min. Then, three 'slow' looming stimuli (36° s^{-1} expansion, as in Figs. 2 and 3), were presented with an inter-trial interval of log delayed times between 90 to 180 s. We used online background subtraction and tracking of mice using Bonsai and stimuli were automatically triggered when the mouse entered a predefined square shaped ROI, covering ~1/3 of the arena, centred on the side opposite to the shelter. Experiments were interrupted early if the mouse sat in the same location for over 20 min. Between each test, the set-up was cleaned thoroughly with 75% ethanol. Each mouse was tested twice, once with CNO and once with saline. The initial condition was randomized. Between the two sessions, mice were undisturbed for 1–2 weeks.

Stimuli. Each looming stimulus trial consisted of 5 successive linear expansions of a black disc on grey background. The disk expanded from an initial ~4° visual angles to ~40° at a rate of 36° s^{-1}. Once it reached full size, the disc maintained its size for 0.5 s, then disappeared and was followed by 0.5 s delay period before entering the next expansion cycle.

Analysis. We followed the same analysis as for visually included behaviour (Figs. 2 and 3). DeepLabCut[73] was used to retrieve centroid coordinates of the mouse. The coordinates of other body parts were used to check for consistency. We calculated the speed of each mouse from these coordinates and smoothed the data using a mean filter with a

width of five frames. We defined and automatically annotated escape events as a speed ≥55.74 cm s^{-1}, and freezing events as a continuous speed of ≤3.28 cm s^{-1} for at least 0.4 s while the mouse was outside the hut.

Ex vivo electrophysiology

Experimental procedure. For whole-cell electrophysiology experiments, coronal slices of dPAG were prepared from 2- to 3-month-old mice. In brief, mice were anaesthetized intraperitoneally with Nembutal (diluted 1:5 in water) and transcardially perfused with ~25 ml of ice-cold *N*-methyl-D-glucamine (NMDG)-based slicing solution containing (in mM): 93 NMDG, 2.5 KCl, 1.2 NaH_2PO_4, 0.5 $CaCl_2$, 10 $MgSO_4$, 30 $NaHCO_3$, 5 sodium ascorbate, 3 sodium pyruvate, 2 thiourea, 20 HEPES and 25 D-glucose (pH adjusted to 7.35 with 10 N HCl, gassed with 95% O_2/5% CO_2). Brains were rapidly extracted and immediately transferred to ice-cold NMDG solution. After removing the rostral part of the brain (Bregma 0.0–0.2 mm) coronal slices (250 µm) were cut from caudal to rostral in ice-cold slicing solution (using a Leica VT1200) and subsequently incubated for ~6 min in the slicing solution at 34 °C for recovery. Afterwards slices were transferred to holding artificial cerebrospinal fluid, containing (in mM): 126 NaCl, 3 KCl, 1 NaH_2PO_4, 1 $CaCl_2$, 6 $MgSO_4$, 26 $NaHCO_3$ and 10 D-glucose (gassed with 95% O_2/5% CO_2). Slices remained at room temperature in holding solution for ~1 h before experiments.

During recordings, brain slices were continuously perfused (32–34 °C) in a submerged chamber (Warner Instruments) at a rate of 3–4 ml min^{-1} with (in mM): 127 NaCl, 2.5 KCl, 1.25 NaH_2PO_4, 25 $NaHCO_3$, 1 $MgCl_2$, 2 $CaCl_2$, 25 glucose at pH 7.4 with 5% CO_2/95% O_2. Whole-cell recordings of dPAG neurons were done using borosilicate glass recording pipettes (resistance 3.5–5 MΩ, Sutter P-1000), using a double EPC-10 amplifier under control of Patchmaster v2 x 32 software (HEKA Elektronik). The following internal medium was used (in mM): 135 potassium gluconate, 4 KCl, 10 HEPES, 4 magnesium ATP, 0.3 sodium GTP, 10 sodium phosphocreatine, 3 biocytin (pH 7.3). Intrinsic properties were recorded in current clamp at 20 Hz and low-pass filtered at 3 kHz when stored. Single action potentials were recorded at 50 Hz and low-pass filtered at 10 kHz. Junction potential was calculated to be approximately 12 mV, data shown are not compensated. For determining neuronal excitability, current injections (−40 pA to +360 pA steps, 10 pA steps) were performed from a holding membrane potential of −70 mV. Rheobase was determined using ramp current injections. For single AP recordings we used conventional bridge balancing and pipette capacitance compensation combined with minimal stimulation intensity to improve separation between AP and stimulation. The series resistance was compensated to 75–80%. Data were analysed using Fitmaster (HEKA Elektronik), spontaneous input was analysed using the Mini Analysis program (Synaptosoft).

Reporting summary

Further information on research design is available in the Nature Portfolio Reporting Summary linked to this article.

Data availability

The source data are available on Dryad (https://doi.org/10.5061/dryad.q2bvq83xc).

Code availability

The code used for the main analyses is available on Dryad (https://doi.org/10.5061/dryad.q2bvq83xc).

61. Brainard, D. H. The psychophysics toolbox. *Spatial Vis.* **10**, 433–436 (1997).
62. Kleiner, M. et al. What's new in psychtoolbox-3. *Perception* **36**, 1–16 (2007).
63. Lenzi, S. C. et al. Threat history controls flexible escape behavior in mice. *Curr. Biol.* **32**, 2972–2979.e2973 (2022).
64. Cardona, A. et al. TrakEM2 software for neural circuit reconstruction. *PLoS ONE* **7**, e38011 (2012).
65. Schindelin, J. et al. Fiji: an open-source platform for biological-image analysis. *Nat. Methods* **9**, 676–682 (2012).
66. Schmidt, U., Weigert, M., Broaddus, C. & Myers, G. Cell detection with star-convex polygons. In *Medical Image Computing and Computer Assisted Intervention—21st International Conference Proceedings Part II* (ed. Frangi, A. F.) 265–273 (Springer, 2018).
67. Jun, J. J. et al. Fully integrated silicon probes for high-density recording of neural activity. *Nature* **551**, 232–236 (2017).
68. Pelli, D. G. The VideoToolbox software for visual psychophysics: transforming numbers into movies. *Spatial Vis.* **10**, 437–442 (1997).
69. Stringer, C., Pachitariu, M., Steinmetz, N., Carandini, M. & Harris, K. D. High-dimensional geometry of population responses in visual cortex. *Nature* **571**, 361–365 (2019).
70. Steinmetz, N. A., Zatka-Haas, P., Carandini, M. & Harris, K. D. Distributed coding of choice, action and engagement across the mouse brain. *Nature* **576**, 266–273 (2019).
71. Ho, J., Tumkaya, T., Aryal, S., Choi, H. & Claridge-Chang, A. Moving beyond *P* values: data analysis with estimation graphics. *Nat. Methods* **16**, 565–566 (2019).
72. Lopes, G. et al. Bonsai: an event-based framework for processing and controlling data streams. *Front. Neuroinformatics* **9**, 7 (2015).
73. Mathis, A. et al. DeepLabCut: markerless pose estimation of user-defined body parts with deep learning. *Nat. Neurosci.* **21**, 1281–1289 (2018).
74. Lopes, G. et al. Creating and controlling visual environments using BonVision. *eLife* **10**, e65541 (2021).

Acknowledgements The authors thank M. Yilmaz, M. Meister, M. Joesch and T. Branco for advice on the behavioural experiments; C. Dulac, V. Bitsikas, E. Diel and J. Chen for advice on the immunohistochemistry and RNAscope experiments; J. Greenwood and E. Soucy for technical and engineering help; A. Chrzanowska for help and advice on optogenetic experiments; A. Calzoni for help aligning histological sections to a brain atlas; S. Worthington for statistical advice; P. Gonçalves for advice with the electrophysiology analysis; I. Vlaemick for help with whole cell experiments; R. Hellmiss for figure design; B. Sabatini, V. Stempel, K. Tyssowski and N. Sanguinetti for feedback on the manuscript; and Y. M. Lee and A. Tomcho for photos of *P. maniculatus* and *P. leucopus* habitats (Fig. 1). F.B. was supported by an HHMI International Student Research Fellowship, a Grant-in-Aid of the American Society of Mammalogy, a Herchel Smith Graduate Fellowship, a Robert A. Chapman Memorial Scholarship, and a Joan Brockman Williamson Fellowship. This project received funding from the European Union's Horizon 2020 research and innovation programme under the Marie Skłodowska-Curie grant agreement 665501 and by the FWO (12S7917N and 12S7920N) to K.R. and from European Research Council (ERC) (grant agreement 101075848) to K.R. V.T. was supported by a Harvard PRISE fellowship and a Harvard Museum of Comparative Zoology grant for undergraduate research. K.F. is supported by the FWO (G094616N and G091719N) and the NIH (1R01EY032101). This work was supported by the Howard Hughes Medical Institute, of which H.E.H. was an Investigator.

Author contributions F.B. and H.E.H. conceived the study. F.B., K.R., K.F. and H.E.H. designed the experiments. F.B. performed the behavioural experiments, with help from V.T. F.B. performed the immunohistochemistry and smFISH experiments. K.R. and B.N. performed the in vivo electrophysiology experiments. K.R. and F.B. performed the optogenetic experiment, with help from J.S.M. A.S.-D. and C.L. performed the chemogenetic experiment. K.W. performed the patch clamp experiment. F.B., K.R., B.N. and K.F. curated and analysed the data. F.B., K.R., K.F. and H.E.H. wrote the paper.

Competing interests The authors declare no competing interests.

Additional information
Supplementary information The online version contains supplementary material available at https://doi.org/10.1038/s41586-025-09241-2.

Correspondence and requests for materials should be addressed to Felix Baier, Karl Farrow or Hopi E. Hoekstra.

Peer review information *Nature* thanks Avishek Adhikari, Cornelius Gross and Philip Tovote for their contribution to the peer review of this work.

Reprints and permissions information is available at http://www.nature.com/reprints.

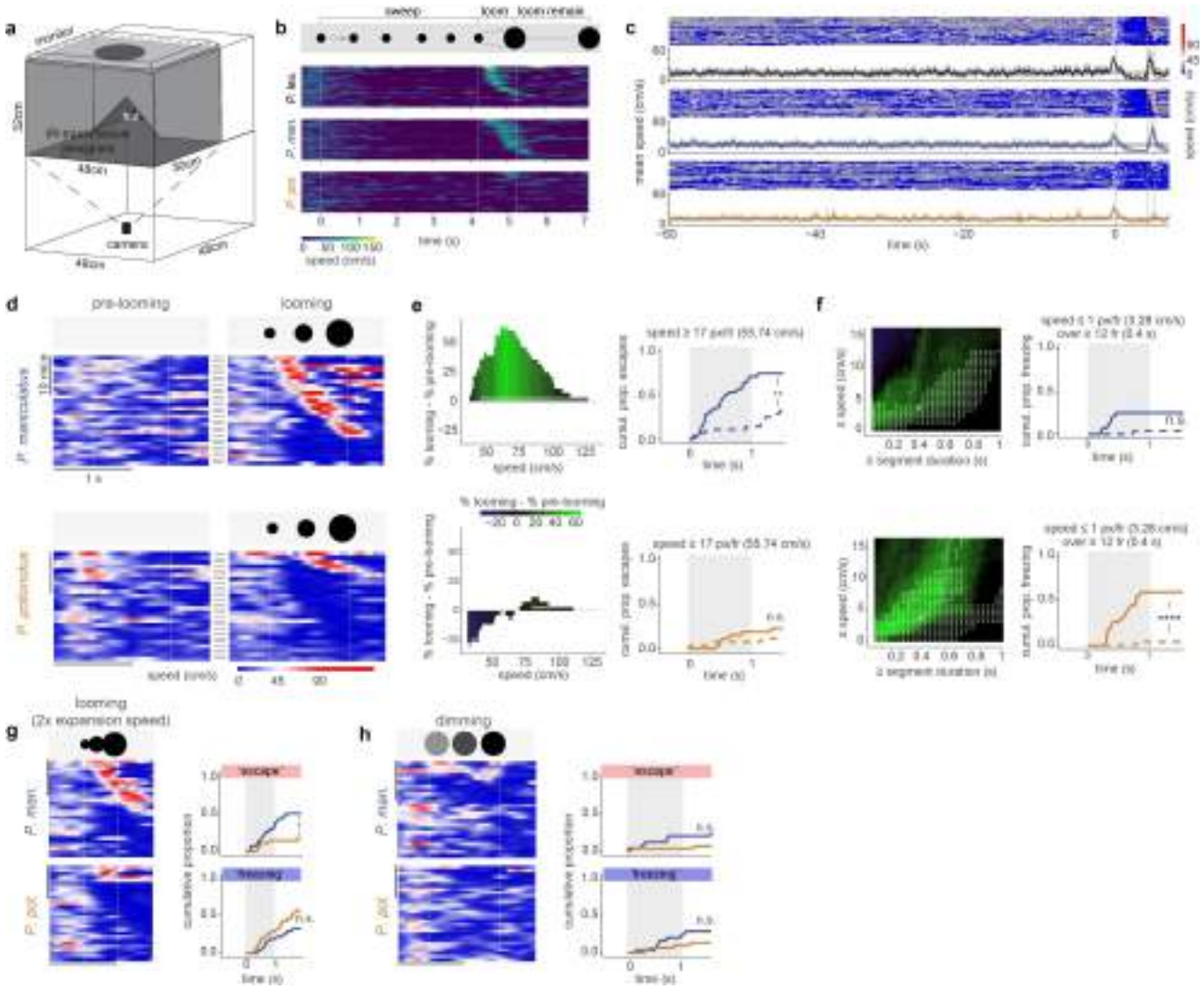

Extended Data Fig. 1 | Quantitative definition of escape and freezing behaviours. (**a**) Arena used to measure behavioural responses to looming stimuli in *Peromyscus* mice. Dimensions for area available to the mouse (grey) and general setup are provided. (**b**) Raster plot showing full range of mouse speed (1–150 cm/s) during the sweep-looming stimulus. (**c**) Raster plots of mouse speed during the 60 s preceding stimulus onset and during the sweep-looming stimulus (top). Rows represent individual mice (*P. leucopus*, n = 28; *P. maniculatus*, n = 29; *P. polionotus*, n = 26). Line plots represent mean speed (solid line) ± 95% confidence limits (color shading), and the 95% confidence interval of the mean speed averaged across the complete 60 s preceding stimulus onset is shaded (horizontal grey bar). (**d**) Raster plots of mouse speed during pre-looming baseline and during looming stimulus approximately 1–2 min later in the same trial. Rows represent individual mice. Speed is represented by a colour gradient. *P. maniculatus* (n = 28), left column; *P. polionotus* (n = 26), right column. The raster plot during the looming stimulus is the same as in Fig. 2d. (**e**) The proportion of mice in (d) that reached a given speed during the looming expansion (1 s) minus the proportion of the same mice that reached the speed during the pre-stimulus control segment (1 s). A positive value indicates that more mice reached a given speed during the stimulus, and a negative value that more mice reached the speed before the stimulus. White dots indicate statistically significant differences between looming-exposed and pre-stimulus proportions. The asterisk indicates the quantitative threshold used to define escape. Based on this threshold, the cumulative proportion of escape during the looming stimulus (highlighted by vertical grey bar; solid line) and the pre-stimulus control segment (dashed line) is shown (right). Sample sizes for *P. maniculatus* (left) and *P. polionotus* (right) are the same as in (d). *P. maniculatus*, $P = 0.003$; *P. polionotus*, $P = 0.464$. (**f**) The proportion of mice in (d) that did not exceed a given speed for a given duration while outside the hut during looming expansion (1 s), minus the equivalent proportion during the pre-stimulus control segment (1 s), as in (e). Based on this definition, the cumulative proportion of freezing during the looming stimulus (as in e) is shown (right). *P. maniculatus*, $P = 0.056$; *P. polionotus*, $P = 4*10^{-5}$. (**g**) Raster plots (left) and cumulative proportion of escape and freezing (right) during a looming stimulus with 2x expansion speed (72°/s). *P. maniculatus* (n = 28); *P. polionotus* (n = 29). Escape, $P = 0.019$; freezing, $P = 0.227$. (**h**) Raster plots (left) and cumulative proportion of escape and freezing during dimming stimulus (right). *P. maniculatus* (n = 25); *P. polionotus* (n = 30). Escape, $P = 0.669$; freezing, $P = 0.175$. For d, g, and h, mice are sorted by onset first of escape and then pausing, with earliest on top. For e, f, g and h, statistical significance was tested with a two-sided Chi-Squared test (cumulative proportion) or Bonferroni-corrected, two-sided binomial test (differences between looming-exposed and pre-stimulus proportions). n.s. not significant; * $P < 0.05$; ** $P < 0.01$; **** $P < 0.0001$.

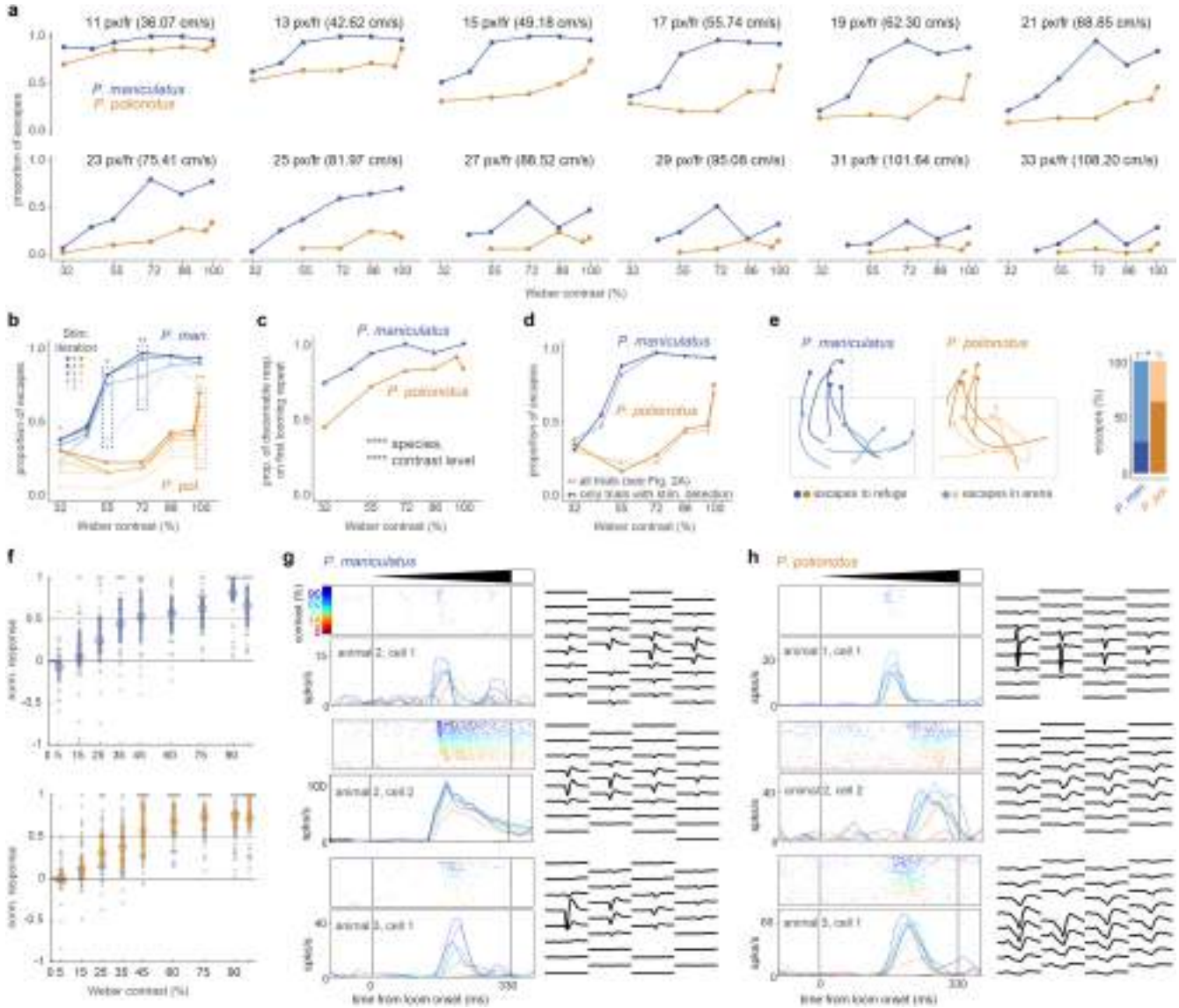

Extended Data Fig. 2 | Cumulative proportion of escape by stimulus repeat, and behavioural and neuronal response rate during contrast experiment. (**a**) Cumulative proportion of escape to visual threat of varying intensity (contrast), for different quantitative escape definitions (11–33 px/fr). The escape cutoff used throughout the paper is 17 px/fr. (**b**) Cumulative proportion of escape by stimulus iteration for *P. maniculatus* (blue) and *P. polionotus* (gold). Dashed boxes indicate contrast levels with statistically significant differences among all five stimulus iterations, and for which the majority of mice had escaped at the end of the last stimulus iteration (*P. maniculatus*, 55% contrast $P = 0.023$, 72% $P = 0.004$; *P. polionotus*, 100% contrast $P = 0.001$). (**c**) Percentage of animals (*P. maniculatus*, blue; *P. polionotus*, gold) in each species that showed a discernible response during the first looming iteration, by contrast level of the looming stimulus (five levels tested for both species; two levels tested in one species). Both contrast level and species have a significant effect on the probability of observing a discernible response (species, $P = 4*10^{-6}$; contrast level, $P = 5*10^{-9}$). (**d**) Comparison of cumulative proportion of escape for all animals (see Fig. 2a; lighter colours) and only those animals that showed a discernible response during the first looming iteration (darker colours). (**e**) Representative trajectories of animals from Fig. 2a (100% contrast) that run around the arena (non-directed escape, lighter colours; n = 5) vs. into the hut (directed escape, darker colours; n = 5). Bar graph showing percentage of escapes around the arena vs. into the hut for each species (right; $P = 0.017$). (**f**) Normalized response strength (0 = baseline activity; 1 = maximum activity) for all responding cells in the sSC for *P. maniculatus* (blue, n = 4) and *P. polionotus* (gold, n = 3) for different Weber contrasts. Circles indicate mean, lines indicate 25–75% of data. (**g-h**) Looming responses of three example cells from the sSC of (g) *P. maniculatus* (n = 3) and (h) *P. polionotus* (n = 3). Raster plots and firing rates (smoothed 20 ms bins) show average response for each contrast (shown in colour code). Waveform footprint (average of 2000 waveforms per cell) on the Neuropixels probe is shown on the right. Statistical significance for proportions was determined by a two-sided Chi-squared test (b) and generalized linear models (c, e). * $P < 0.05$; ** $P < 0.01$; **** $P < 0.0001$.

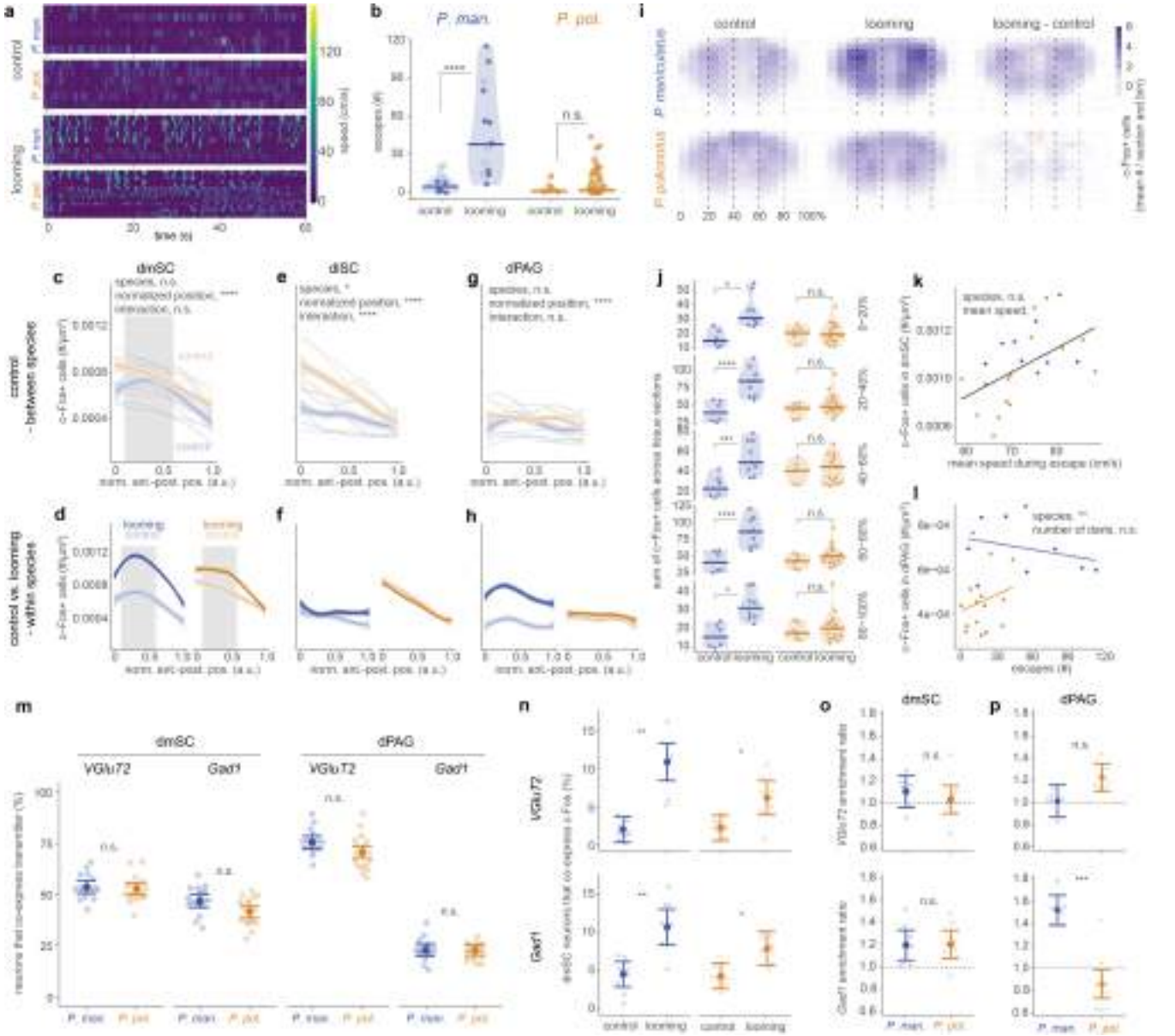

Extended Data Fig. 3 | Additional information about c-Fos experiment. (**a**) Raster plot of speed of animals in control (n = 6 each species) and looming (first 60 s following looming onset; *P. maniculatus*, n = 9; *P. polionotus*, n = 15) assays included in the c-Fos analysis (shown in Fig. 3b). Dashed line indicates stimulus onset. (**b**) Number of escapes of *P. maniculatus* (blue) and *P. polionotus* (gold). Filled circles indicate data included in the c-Fos experiment (looming, *P. maniculatus*, n = 9; *P. polionotus*, n = 15; control, n = 6 for both species). Statistical significance was tested with a linear mixed effects model (*P. maniculatus*, $P = 0.0$; *P. polionotus*, $P = 0.283$). (**c**) Number of c-Fos+ cells in control mice of both species (*P. maniculatus*, blue; *P. polionotus*, gold) along anterior-posterior position in dmSC. Lines represent individual mice (thin), mean per species (thick) and 95% CI (shading). Statistical significance was tested with a linear mixed effects model, including animal ID as a random effect (species, $P = 0.254$; normalized position, $P < 1*10^{-4}$; interaction, $P = 0.393$). (**d**) Number of c-Fos+ cells in control and looming-exposed mice along anterior-posterior position of dmSC. Levels in looming-exposed mice are maximized in the central dmSC (highlighted in grey boxes). The sections within the grey boxes were used for the analyses in Fig. 3. (**e**) Same as (c), but for dlSC (species, $P = 0.034$; normalized position, $P < 1*10^{-4}$; interaction, $P < 1*10^{-4}$). (**f**). Same as (d), but for dlSC. (**g**) Same as (c), but for dPAG (species, $P = 0.4810$; normalized position, $P < 1*10^{-4}$; interaction, $P = 0.674$). (**h**) Same as (d), but for dPAG. Statistical significance was tested with a linear mixed effects model. (**i**) Heatmaps of mean number of c-Fos+ cells per spatial bin across the dPAG, averaged across sections and animals, in control and looming-exposed animals and their difference. (**j**) Quantification of c-Fos+ cells for the coronal ranges indicated with dashed lines in i. Statistical significance was tested with a linear mixed effects model (*P. maniculatus*, 0–20% $P = 0.014$, 20–40% $P = 3*10^{-6}$, 40–60% $P = 4*10^{-4}$, 60–80% $P = 2*10^{-6}$, 80–100% $P = 0.026$; *P. polionotus*, 0–20% $P = 0.845$, 20–40% $P = 0.347$, 40–60% $P = 0.845$, 60–80% $P = 0.347$, 80–100% $P = 0.845$). (**k**) Number of c-Fos+ cells in the dmSC as a function of mean speed during escape (*P. maniculatus*, n = 9; *P. polionotus*, n = 14). Statistical significance was tested with a linear fixed effects model (species, $P = 0.064$; mean speed, $P = 0.015$). (**l**) Number of c-Fos+ cells in the dPAG as a function of the number of escapes. Statistical significance was tested with a linear fixed effects model (species, $P = 0.002$; number of escapes, $P = 0.741$). (**m**) Proportion of excitatory (*VGluT2* +) and inhibitory (*Gad1* +) neurons in dmSC and dPAG. (**n**) Proportion of c-Fos+ excitatory (top) and inhibitory (bottom) dmSC neurons in control and looming-exposed mice (VGluT2, *P. maniculatus* $P = 0.002$, *P. polionotus* $P = 0.032$; Gad1, *P. maniculatus* $P = 0.006$, *P. polionotus* $P = 0.039$). (**o**) Enrichment index [proportion of excitatory/inhibitory neurons that co-express c-Fos, divided by the overall proportion of c-Fos+ neurons] for excitatory (top) and inhibitory (bottom) neurons in dmSC of looming-exposed mice (VGluT2, $P = 0.773$; Gad1, $P = 0.939$). (**p**) Enrichment index for excitatory (top) and inhibitory (bottom) neurons in dPAG (VGluT2, $P = 0.255$; Gad1, $P = 8*10^{-4}$). Statistical significance in m-p was determined by a linear mixed effects model. n.s. not significant; * $P < 0.05$; ** $P < 0.01$; **** $P < 0.0001$.

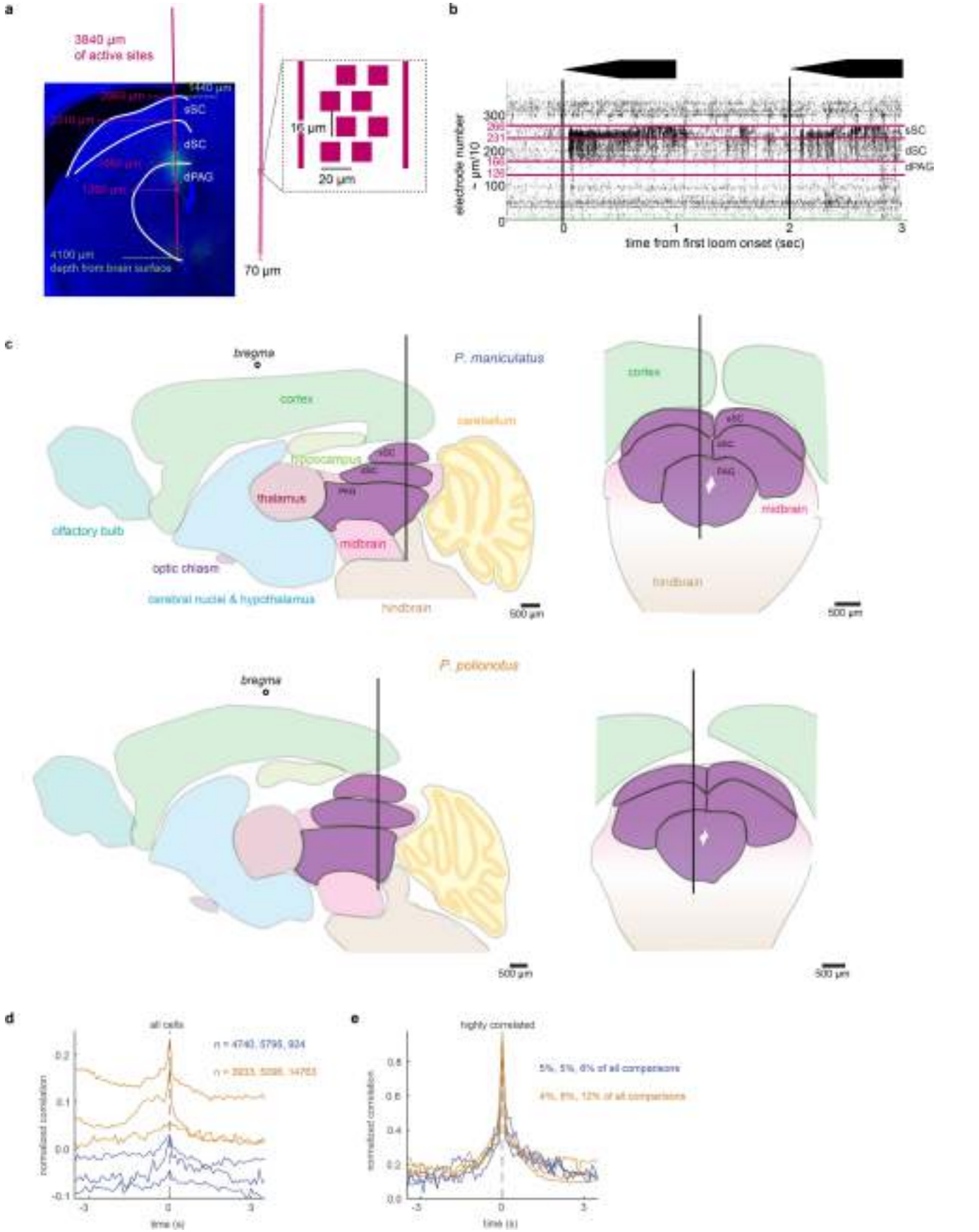

Extended Data Fig. 4 | See next page for caption.

Extended Data Fig. 4 | Detailed methods for the Neuropixels recordings. (**a**) Histological image of a coronal slice through the SC and PAG. Magenta line indicates the location of the Neuropixels probe that had been coated with a dye (DiI). White lines indicate separation between sSC, dSC and PAG based on inspection of the brain slice and activity patterns. Magenta numbers indicate depth from the tip of the probe; green numbers indicate depth from the brain surface. Right: Bottom portion of Neuropixels probe (total: 960 electrodes) shown at the same scale as the histological image. Zoomed-in version shows positioning of individual electrodes (magenta squares). (**b**) Example raw spiking activity during two loom stimuli of the same animal as in A. Numbers indicate depth from probe tip, magenta numbers correspond to borders in A. Histological assessment together with raw spiking activity patterns were used to identify sSC, dSC and dPAG borders. See Methods for details. (**c**) Outlines of two sagittal and coronal slices traced from histological slices from the two species. Major brain areas were estimated based on DAPI staining and comparison to the *Mus* brain atlases as well as choleratoxin-B injections into the *Peromyscus* eye (data not shown). Representative placement of the Neuropixels probe is indicated as well as the anterior-posterior position of bregma for sagittal sections. Adapted from Allen Mouse Brain Atlas (mouse.brain-map.org and atlas.brain-map.org). (**d**) Average normalized cross-correlation of all recorded activity in the dSC and dPAG. The number of comparisons (cells in dSC vs cells in dPAG) for each animal (*P. maniculatus*, blue; *P. polionotus*, gold; n = 3 for each species) is shown. (**e**) Average normalized cross-correlation of all dSC and dPAG comparisons with a correlation coefficient > 0.8 ("highly correlated"). Percentages indicate the fraction of all comparisons that fulfilled the criterion of highly correlated activity for each animal.

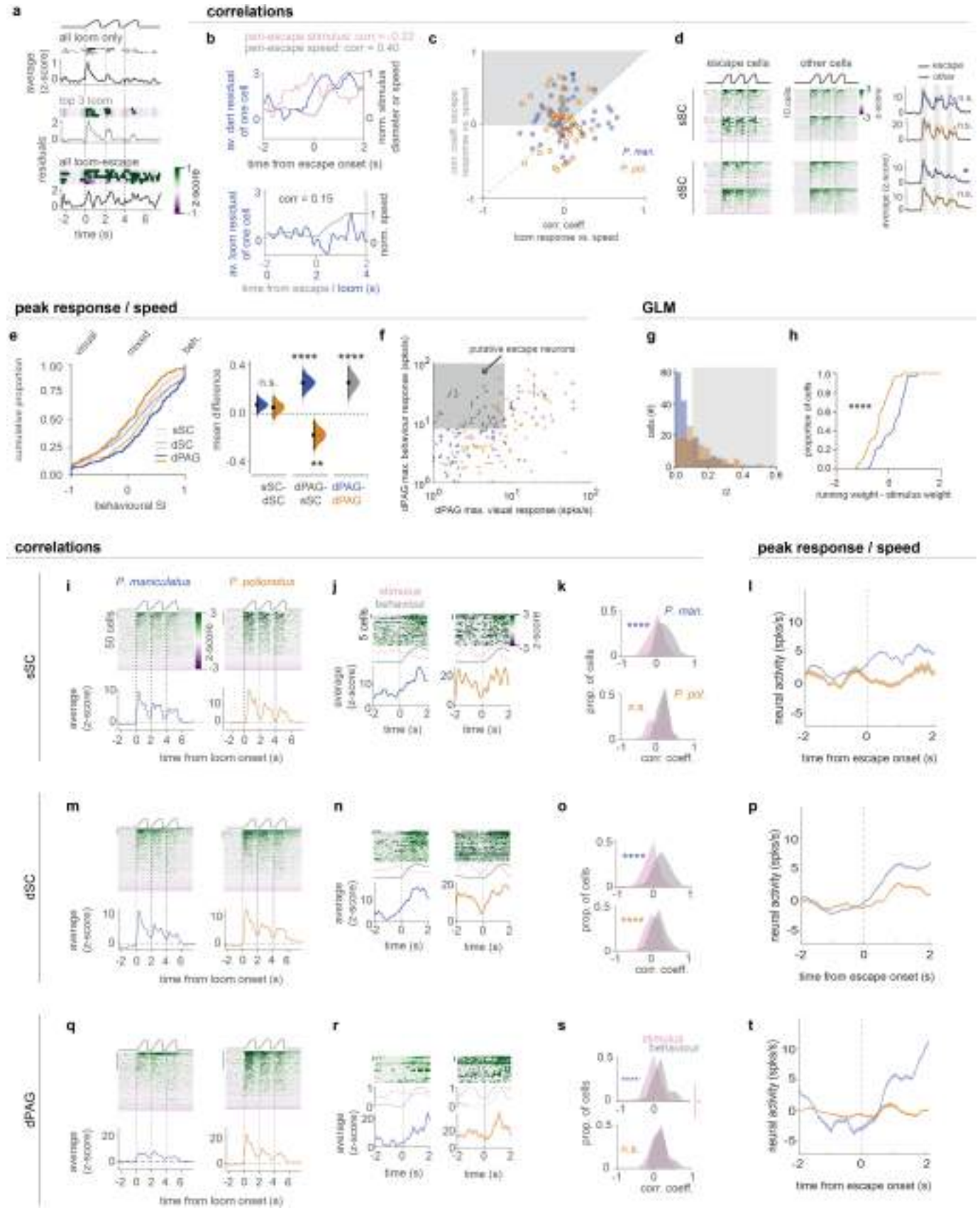

Extended Data Fig. 5 | See next page for caption.

Extended Data Fig. 5 | Locomotory and neural activity in the immersive setup. (**a**) Example of template and residual calculation. Top: average response of one cell to all looms without escapes. Middle: heatmap of three residuals from trials with strongest stimulus correlation during non-escape looms and average of those residuals. Bottom: heatmap of all residuals during looming stimuli followed by escapes and averages of those residuals. (**b**) Top: Example Spearman correlation of residual neural activity (blue) with running speed (grey; Cb; see Methods) and peri-escape visual stimulus diameter (rose; Cp). Bottom: Example correlation of neural activity during the first loom without escapes (blue) with running speed during escapes (grey; Cn). (**c**) Cn (x-axis) and Cb (y-axis) were compared to identify putative escape neurons. Only neurons for which the correlation of escape speed with the corresponding neural activity (y-axis) was positive and larger than the correlation of escape speed with the neural activity during a non-escape loom (x-axis) were included in further analysis (grey shaded area). (**d**) Responses of putative escape cells (left) and all other cells (middle) in the absence of escape. Mean ± SEM (blue/gold: putative escape cells; black: other cells) (right). Statistics compare mean response during first loom. sSC: *P. maniculatus* $P = 0.345$; *P. polionotus* $P = 0.206$. dSC: *P. maniculatus* $P = 0.028$; *P. polionotus* $P = 0.284$. (**e**) Behavioural selectivity index (SI) calculated based on maximum firing rates during escape peak instead of correlations coefficients (left) and estimation statistics of the same data (right). Dots indicate means, lines indicate 95% confidence intervals. The same data as in Fig. 5 was used. sSC: 538 cells from n = 6 *P. maniculatus* animals; 254 cells from n = 4 *P. polionotus* animals. dSC: 574 cells from n = 6 *P. maniculatus* animals; 413 cells from n = 4 *P. polionotus* animals. dPAG: 169 cells from n = 6 *P. maniculatus* animals; 143 cells from n = 4 *P. polionotus* animals. sSC-dSC: *P. maniculatus* $P = 0.062$; *P. polionotus* $P = 0.321$. dPAG-sSC: *P. maniculatus* $P < 0.0001$; *P. polionotus* $P = 0.004$. dPAG across species: $P < 0.0001$. (**f**) Scatter plot of maximum firing rates during the first loom of visual-only trials and during escape behaviours. Grey area indicates putative escape neurons with a maximum behavioural firing rate > mean(escape firing rates of all cells) && maximum visual firing rate <mean(escape firing rates of all cells). (**g**) Histogram of combined explained variance using visual and running trials (r2). Cells with r2 > 0.1 were included in panel h and Fig. 4g,h. (**h**) Cumulative distribution of the difference between running and stimulus weights from Fig. 4g. $P = 6*10^{-5}$. Data was binned in 500 ms bins; different bins sizes led to qualitatively and quantitatively similar results for this analysis as well as Fig. 4h. Relative explained variance (Fig. 4h): 1 s: $P = 3*10^{-6}$; 1.5 s: $P = 3*10^{-7}$; 2 s: $P = 9*10^{-8}$. Differences of weights (this panel h): 1 s: $P = 3*10^{-5}$; 1.5 s: $P = 4*10^{-5}$; 2 s: $P = 0.005$. (**i**) Heatmaps of average responses of all sSC neurons to looming stimuli, in the absence of escape (top). Average z-score ± SEM (bottom). (**j**) Neural activity of putative escape neurons during escapes (heatmaps and averages in blue/gold), average running speed during escape (grey) and average peri-escape visual stimulus diameter (pink). (**k**) Correlation of neural activity during escapes with speed (grey) and peri-escape visual stimulus (pink). *P. maniculatus* $P = 5*10^{-5}$; *P. polionotus* $P = 0.383$. (**l**) Mean ± SEM firing peri-escape neural activity of putative escape neurons based on peak response (see f). (**m**-**p**) Same plots for dSC neurons. *P. maniculatus* $P = 2*10^{-14}$; *P. polionotus* $P = 2*10^{-4}$. (**q**-**t**) Same plots for dPAG neurons. *P. maniculatus* $P = 5*10^{-4}$; *P. polionotus* $P = 0.124$. Statistical significance evaluated with two-sided unpaired mean difference Gardner-Altman estimation (e right), two-sided Brunner-Munzel test (d) and two-sided, two-sample Kolmogorov-Smirnov test (h, k, o, s). n.s. not significant; ** $P < 0.01$; **** $P < 0.0001$.

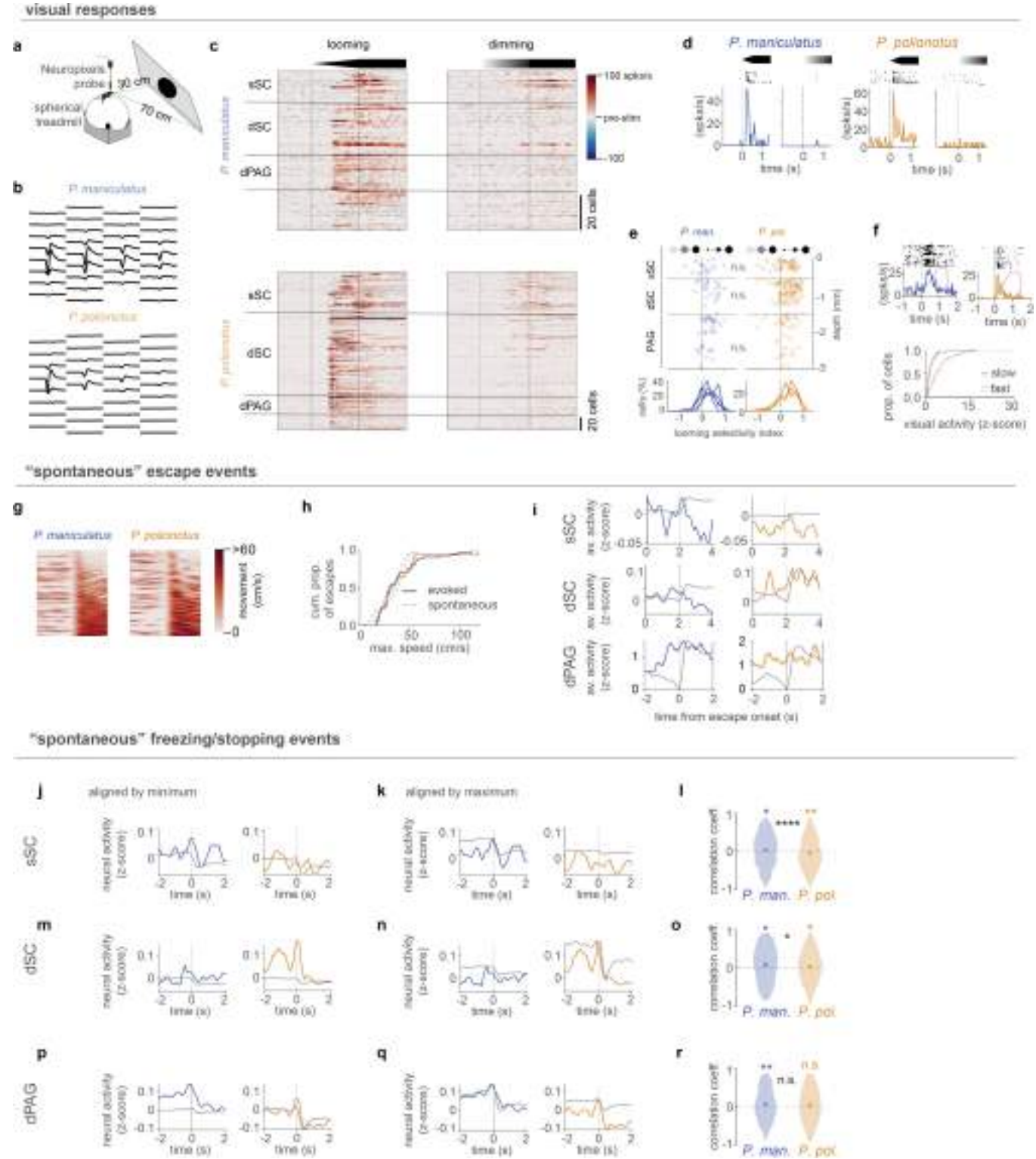

Extended Data Fig. 6 | See next page for caption.

Extended Data Fig. 6 | Locomotory and neural activity in the monitor setup. (**a**) Setup used to record neural activity during spontaneous escapes and stops. (**b**) Waveform footprint (average of 2000 waveforms per cell) on the Neuropixels probe of example cells from *P. maniculatus* (top) and *P. polionotus* (bottom) shown in panel d. (**c**) Average, background-subtracted looming (left) and dimming (right) response for all recorded cells shown in panel e. Cells are sorted by depth; the same rows for looming and dimming correspond to the same cell. (**d**) Example responses to dimming and fast looming (330 ms) stimuli of one cell per species recorded on the setup shown in a. Top: raster plots. Bottom: Average firing rates. (**e**) Selectivity of looming vs. dimming response (top). Distribution of looming selectivity for each animal (*P. maniculatus*, n = 4 animals; *P. polionotus*, n = 3) (bottom). (**f**) Top: Example response to a slow looming stimulus (1 s) recorded on the immersive setup in Fig. 4a. Rose: corresponding visual stimulus diameter. Bottom: Peak response (z-score) for slow looms recorded in the immersive setup (solid lines) and for fast looms recorded on the monitor setup (dashed lines). (**g**) Speed during spontaneous escape events, separated by species. (**h**) Maximum speed during evoked and spontaneous escape events for *P. maniculatus* (blue) and *P. polionotus* (gold). (**i**) Average activity during spontaneous escapes (blue and gold) and average speed during escapes (grey) for neurons with max. z-score >4 STD. Speed traces aligned with z-score of 0 before escape and with maximum during escape to highlight neurons that respond to the escape. (**j**) Average sSC activity during spontaneous stops (blue and gold) and average speed during stops (grey). Speed traces aligned with z-score of 0 before stop and with minimum during stop to highlight neurons that respond to the stop. (**k**) Same plot as in j but speed trace aligned with maximum neural activity before stop and 0 z-score during stop to highlight neurons that respond to running speed. *P. maniculatus* neurons appear to be active during running and return to baseline firing during stop. *P. polionotus* neurons tend to react to stopping behaviour by inhibition. (**l**) Correlation coefficient of stop speed traces and corresponding neural activity. *P. maniculatus* $P = 0.020$; *P. polionotus* $P = 0.001$; across species $P = 1*10^{-6}$. (**m-o**) Same as j-l for dSC neurons. dSC neurons are likely composed of a mixed group of types that encode running or stopping. *P. maniculatus* $P = 0.010$; *P. polionotus* $P = 0.010$; across species $P = 0.010$. (**p-r**) Same as j-l for dPAG neurons. No clear relationship with behaviour is apparent. *P. maniculatus* $P = 0.001$; *P. polionotus* $P = 0.075$; across species $P = 0.475$. Statistical significance for all comparisons was evaluated with two-sided, two-sample Kolmogorov-Smirnov test. n.s. not significant; * $P < 0.05$; ** $P < 0.01$; **** $P < 0.0001$.

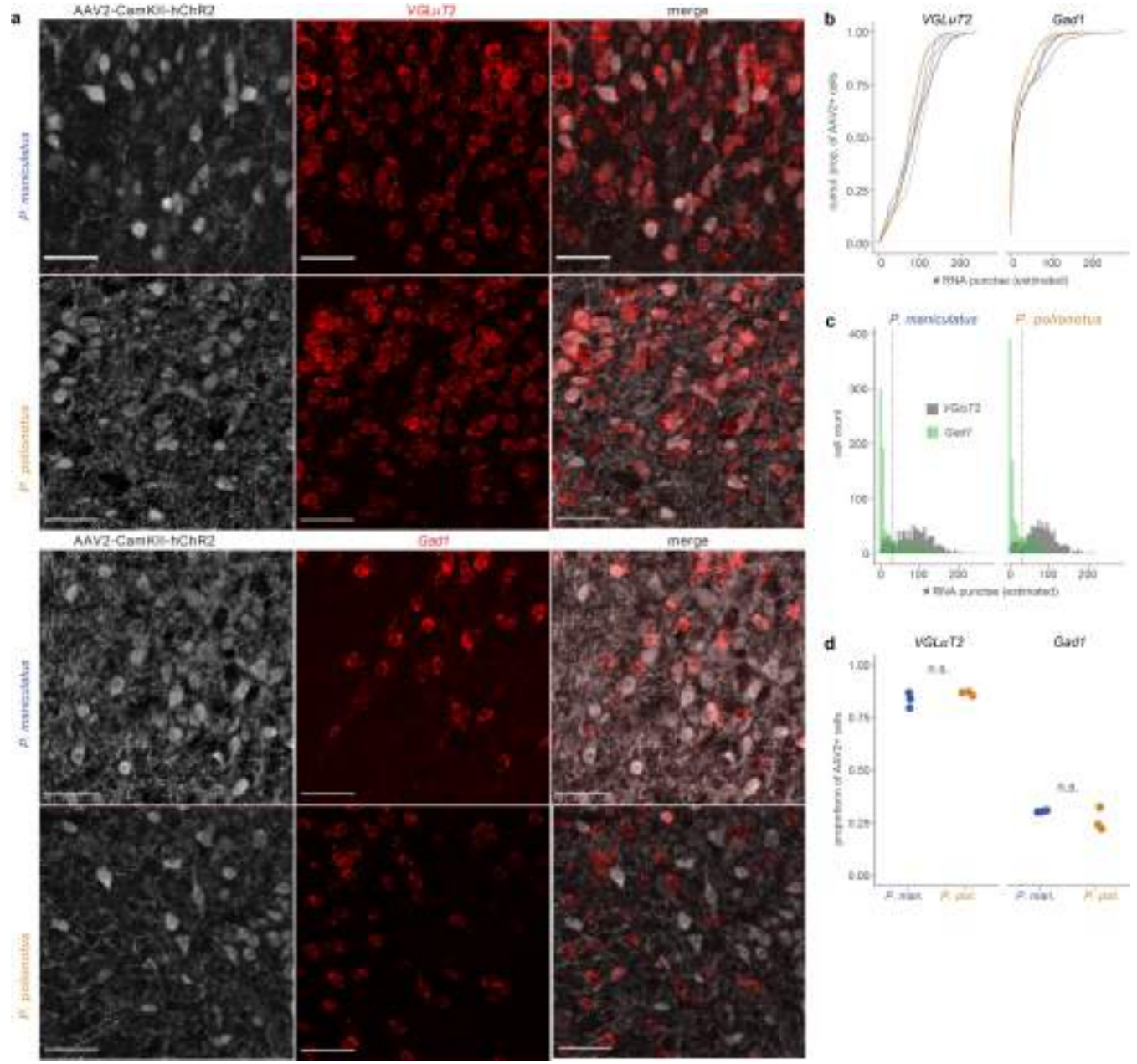

Extended Data Fig. 7 | Single-molecule FISH quantification of AAV infection patterns. (**a**) Representative images of AAV2 expression and RNAscope probes against *VGluT2* (excitatory; top) and *Gad1* (inhibitory; below) for *P. maniculatus* and *P. polionotus*. Scale bar, 50 µm. (**b**) Cumulative proportion of AAV2+ cells by estimated number of RNA punctae for *VGluT2* (left) and *Gad1* (right). Individual lines represent animals (n = 3, per species). (**c**) Distribution of RNA punctae across excitatory/inhibitory cells. Cut-off for assigning cell identity is indicated by the dashed line. (**d**) Percentage of AAV2+ cells that express *VGluT2* (excitatory; left) or *Gad1* (inhibitory; right) in both species. Statistical significance was tested with a linear fixed effects model. n.s. not significant.

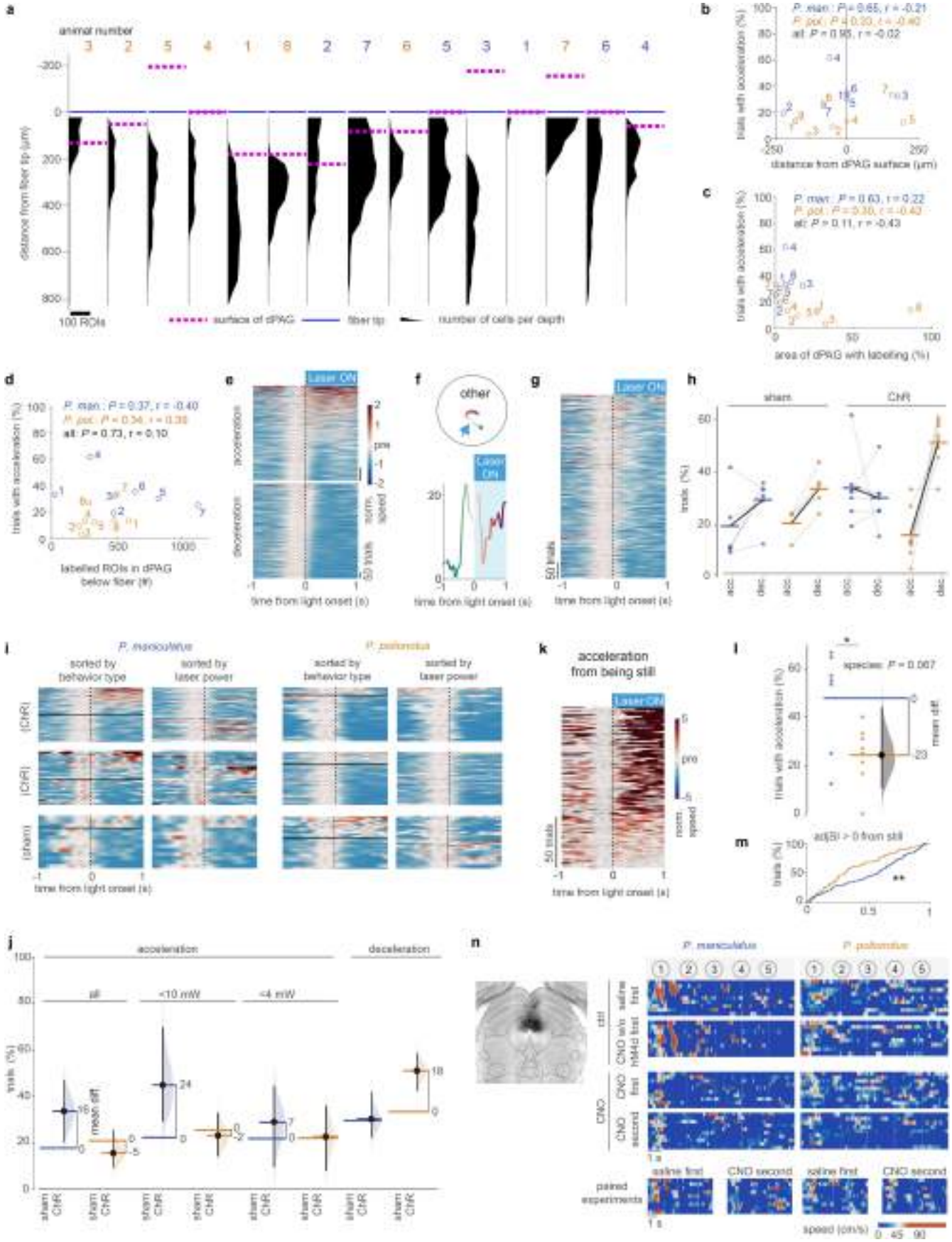

Extended Data Fig. 8 | See next page for caption.

Extended Data Fig. 8 | Quantification of channelrhodopsin (ChR2)-positive cells, fibre placement, and behavioural classification. (**a**) Distribution of YFP-positive regions of interest (ROIs; presumably cells) below the fibre tip. Dashed lines (magenta) indicate the surface of the dPAG; blue lines indicate the fibre tip. Animals were sorted by increasing percentage of running trials (data from Fig. 5i); animal ID numbers are provided (*P. maniculatus*, blue; *P. polionotus*, gold). (**b**) Fibre location relative to the dPAG surface and % of trials with observed acceleration behaviour. (**c**) Percentage of fluorescently labelled dPAG area and % of trials with observed acceleration behaviour. (**d**) Number of labelled ROIs (presumably cells) in the dPAG below the fibre and % of trials with observed acceleration behaviour. (**e**) Data from Fig. 5c, but only showing acceleration and deceleration trials. (**f**) Example trajectory and speed trace of behaviour classified as "Other". (**g**) All traces from both species classified as "Other". (**h**) Comparison of acceleration and deceleration trials per animal (*P.* maniculatus: ChR n = 7 animals, sham n = 6; *P. polionotus*: ChR n = 8, sham n = 5). Horizontal lines indicate means. (**i**) All optogenetics trials for three (two ChR and one sham) example *P. maniculatus* and *P. polionotus* animals. Left and right column for each species represents the same data, but sorted by speed (left) or by laser power (right; starting from lowest to highest). (**j**) Mean difference (black dot) and confidence intervals (vertical black line) for the data from Fig. 5g-i extracted from estimation statistics (unpaired mean difference Gardner-Altman estimation); distribution represents 5000 bootstrapped samples. (**k**) Heatmap of all trials with acceleration from being still, normalized to 0.37 s before laser onset. (**l**) Comparison of trials with acceleration from being still for *P. maniculatus* and *P. polionotus* animals. ANOVA test results of interaction between species and acceleration ($P = 0.067$). Not enough movement from still trials could be collected for sham animals. (**m**) Cumulative distribution of adjusted Speed Index (SI, see also Extended Data Fig. 9) for acceleration trials from being still. $P = 0.001$. (**n**) Left: Representative example of hM4d(gi)-mCherry expression (black) in the dPAG. Outlines correspond to estimated borders based on *Mus* brain atlas. Adapted from Allen Mouse Brain Atlas (mouse.brain-map.org and atlas.brain-map.org). Right: Heatmaps of speed during five looming stimuli for control trials (Fig. 5m: hM4d(gi) + saline, top; mCherry + CNO, bottom) and CNO trials (Fig. 5m: hM4d(gi) + CNO as first session, top; or as second session, bottom). Only the first exposures to the looming stimulus were included in control trials. Bottom: subset of trials from animals that underwent an hM4d(gi) + saline first session followed one week later by a hM4d(gi) + CNO session. Rows correspond to the same animal. Statistical significance evaluated with unpaired mean difference Gardner-Altman estimation (l) and two-sided, two-sample Kolmogorov-Smirnov test (m). * $P < 0.05$; ** $P < 0.01$.

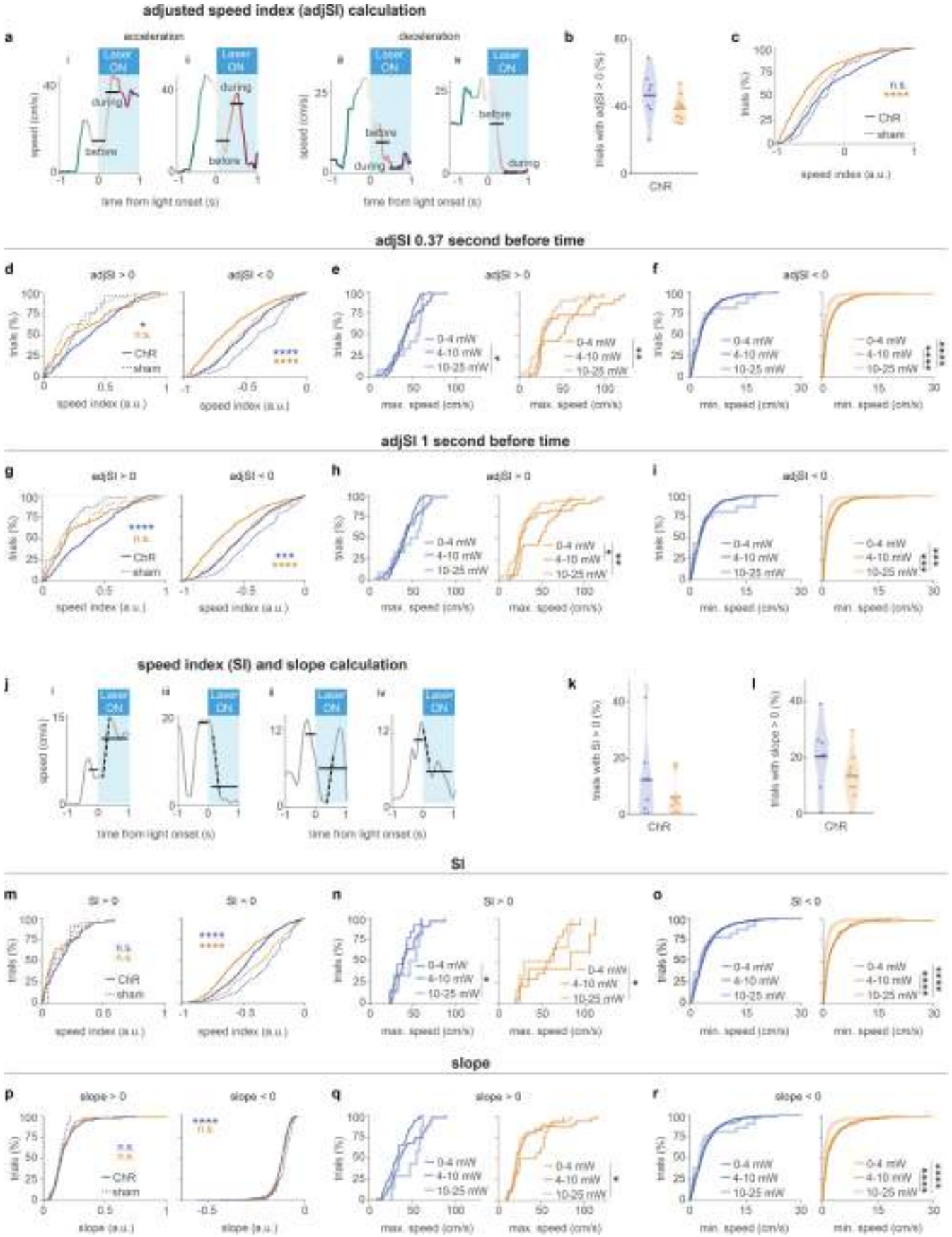

Extended Data Fig. 9 | See next page for caption.

Extended Data Fig. 9 | Various analysis strategies of optogenetically induced behaviour. (**a-i**) Adjusted Speed Index (adjSI). (**a**) For adjusted SI calculation, the extrema during the laser triggers were found. Five frames around the extremum were used to calculate the elicited behaviour ('during'). Five frames around the preceding maximum/minimum were used to calculate the baseline ('before'). The speed index was calculated as ([speed before] − [speed during])/([speed before] + [speed during]). (**b**) Trials with adjSI > 0 (i.e., acceleration) in *P. maniculatus* (blue, n = 7 animals) and *P. polionotus* (gold, n = 8). (**c**) adjSI distributions for ChR and sham animals of both species. (**d**) Cumulative distributions for adjSI > 0 (acceleration; *P. maniculatus* $P = 0.024$; *P. polionotus* $P = 0.237$) and adjSI <0 (deceleration; *P. maniculatus* $P = 2*10^{-4}$; *P. polionotus* $P = 7*10^{-8}$). (**e**) Maximum running speed for adjSI > 0 trials at different laser powers for *P. maniculatus* and *P. polionotus*. <4 vs <10 mW: *P. maniculatus* $P = 0.085$, *P. polionotus* $P = 0.195$; <4 vs <25 mW: *P. maniculatus* $P = 0.017$, *P. polionotus* $P = 0.009$; <10 vs <25 mW: *P. maniculatus* $P = 0.192$, *P. polionotus* $P = 0.277$. (**f**) Minimum running speed for adjSI <0 trials at different laser powers. <4 vs <10 mW: *P. maniculatus* $P = 0.164$, *P. polionotus* $P = 0.953$; <4 vs <25 mW: *P. maniculatus* $P = 0.211$, *P. polionotus* $P = 1*10^{-9}$; <10 vs <25 mW: *P. maniculatus* $P = 0.842$, *P. polionotus* $P = 4*10^{-7}$. (**g-i**) Similar results were found when 1 s was used for baseline ('before') measurements. (g) Acceleration: *P. maniculatus* $P = 5*10^{-5}$; *P. polionotus* $P = 0.367$. Deceleration: *P. maniculatus* $P = 0.004$; *P. polionotus* $P = 1*10^{-8}$. (h) <4 vs <10 mW: *P. maniculatus* $P = 0.144$, *P. polionotus* $P = 0.020$; <4 vs <25 mW: *P. maniculatus* $P = 0.094$, *P. polionotus* $P = 0.004$; <10 vs <25 mW: *P. maniculatus* $P = 0.414$, *P. polionotus* $P = 0.474$. (i) <4 vs <10 mW: *P. maniculatus* $P = 0.992$, *P. polionotus* $P = 1.000$; <4 vs <25 mW: *P. maniculatus* $P = 0.945$, *P. polionotus* $P = 0.004$; <10 vs <25 mW: *P. maniculatus* $P = 1.000$, *P. polionotus* $P = 0.002$. (**j-r**) Additional analysis considering two different parameters – non-adjusted SI and slope. (**j**) For the SI, the speed during the laser trigger was compared to the speed during 0.37 s right before laser onset (solid lines). The speed index was calculated as ([speed before] − [speed during])/([speed before] + [speed during]). For slope measurements, the slope was calculated in sliding windows and the maximum slope was taken (dashed lines). (**k-l**) Comparison of acceleration trials (SI > 0 or slope > 0) for the two species (*P. maniculatus:* n = 7 animals; *P. polionotus:* n = 8). (**m**) Cumulative distributions of speed indices <0 and >0. Acceleration: *P. maniculatus* $P = 0.747$; *P. polionotus* $P = 0.907$. Deceleration: *P. maniculatus* $P = 4*10^{-10}$; *P. polionotus* $P = 5*10^{-10}$. (**n**) Maximum speed for SI > 0 trials at different laser powers. <4 vs <10 mW: *P. maniculatus* $P = 0.090$, *P. polionotus* $P = 0.071$; <4 vs <25 mW: *P. maniculatus* $P = 0.070$, *P. polionotus* $P = 0.035$; <10 vs <25 mW: *P. maniculatus* $P = 0.0357$, *P. polionotus* $P = 0.373$. (i) <4 vs <10 mW: *P. maniculatus* $P = 0.992$, *P. polionotus* $P = 1.000$; <4 vs <25 mW: *P. maniculatus* $P = 0.945$, *P. polionotus* $P = 0.004$; <10 vs <25 mW: *P. maniculatus* $P = 1.000$, *P. polionotus* $P = 0.002$. (**o**) Minimum speed for SI < 0 trials at different laser powers. <4 vs <10 mW: *P. maniculatus* $P = 0.103$, *P. polionotus* $P = 0.994$; <4 vs <25 mW: *P. maniculatus* $P = 0.324$, *P. polionotus* $P = 3*10^{-10}$; <10 vs <25 mW: *P. maniculatus* $P = 0.751$, *P. polionotus* $P = 7*10^{-8}$. (i) <4 vs <10 mW: *P. maniculatus* $P = 0.992$, *P. polionotus* $P = 1.000$; <4 vs <25 mW: *P. maniculatus* $P = 0.945$, *P. polionotus* $P = 0.004$; <10 vs <25 mW: *P. maniculatus* $P = 1.000$, *P. polionotus* $P = 0.002$. (**p-r**) Same plots as m-o for slope parameter. (p) Acceleration: *P. maniculatus* $P = 0.201$; *P. polionotus* $P = 0.989$. Deceleration: *P. maniculatus* $P = 5*10^{-5}$; *P. polionotus* $P = 0.605$. (q) <4 vs <10 mW: *P. maniculatus* $P = 0.090$, *P. polionotus* $P = 0.071$; <4 vs <25 mW: *P. maniculatus* $P = 0.070$, *P. polionotus* $P = 0.035$; <10 vs <25 mW: *P. maniculatus* $P = 0.357$, *P. polionotus* $P = 0.373$. (i) <4 vs <10 mW: *P. maniculatus* $P = 0.082$, *P. polionotus* $P = 0.476$; <4 vs <25 mW: *P. maniculatus* $P = 0.278$, *P. polionotus* $P = 5*10^{-11}$; <10 vs <25 mW: *P. maniculatus* $P = 0.820$, *P. polionotus* $P = 2*10^{-7}$. Statistical significance for all comparisons was evaluated with two-sided, two-sample Kolmogorov-Smirnov test. * $P < 0.05$, ** $P < 0.01$, *** $P < 0.005$, **** $P < 0.0001$.

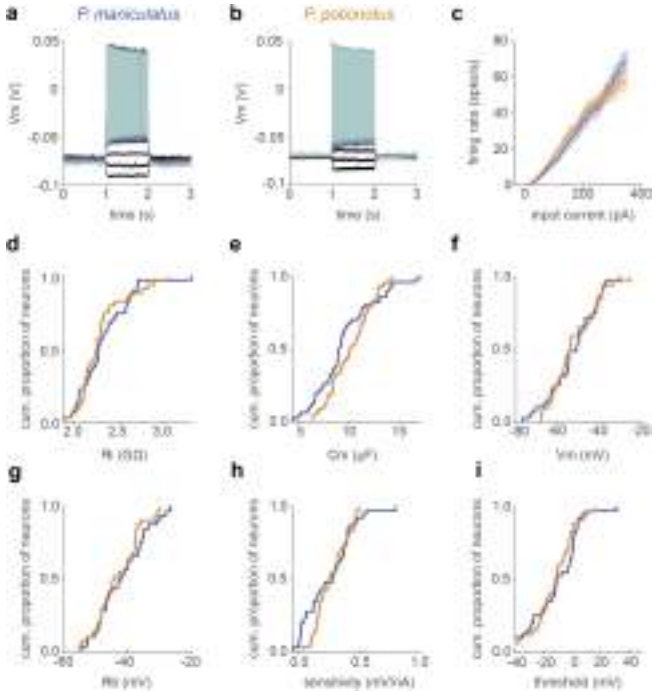

Extended Data Fig. 10 | In vitro patch clamp assessment of intrinsic properties of neurons in the dPAG. (**a**-**b**) Example current clamp experiments in the dPAG of brains slices from *P. maniculatus* (**a**) and *P. polionotus* (**b**). Current was injected in steps of 10 nA from −40 to 350 nA. (**c**). Average current firing rate (± SEM) curves of dPAG neurons in *P. maniculatus* (blue, n = 52 neurons) and *P. polionotus* (gold, n = 47 neurons). (**d-i**) Distribution of intrinsic parameters measured from current clamp experiments of dPAG neurons in *P. maniculatus* (blue, n = 52 neurons) and *P. polionotus* (gold, n = 47 neurons). (**d**) Input resistance ($P = 0.60$). (**e**) Membrane capacitance ($P = 0.15$). (**f**) Membrane potential ($P = 0.88$). (**g**) Rheobase ($P = 0.42$). (**h**) Firing rate sensitivity ($P = 0.18$). (**i**) Firing rate threshold ($P = 0.38$). Statistical significance evaluated with two-sided, two-sample Kolmogorov-Smirnov test. All statistical comparisons were not significant ($P > 0.05$).

nature portfolio

Corresponding author(s): Hopi E. Hoekstra

Last updated by author(s): May 13, 2025

Reporting Summary

Nature Portfolio wishes to improve the reproducibility of the work that we publish. This form provides structure for consistency and transparency in reporting. For further information on Nature Portfolio policies, see our Editorial Policies and the Editorial Policy Checklist.

Statistics

For all statistical analyses, confirm that the following items are present in the figure legend, table legend, main text, or Methods section.

n/a	Confirmed
☐	☒ The exact sample size (*n*) for each experimental group/condition, given as a discrete number and unit of measurement
☐	☒ A statement on whether measurements were taken from distinct samples or whether the same sample was measured repeatedly
☐	☒ The statistical test(s) used AND whether they are one- or two-sided *Only common tests should be described solely by name; describe more complex techniques in the Methods section.*
☐	☒ A description of all covariates tested
☐	☒ A description of any assumptions or corrections, such as tests of normality and adjustment for multiple comparisons
☐	☒ A full description of the statistical parameters including central tendency (e.g. means) or other basic estimates (e.g. regression coefficient) AND variation (e.g. standard deviation) or associated estimates of uncertainty (e.g. confidence intervals)
☐	☒ For null hypothesis testing, the test statistic (e.g. *F*, *t*, *r*) with confidence intervals, effect sizes, degrees of freedom and *P* value noted *Give P values as exact values whenever suitable.*
☒	☐ For Bayesian analysis, information on the choice of priors and Markov chain Monte Carlo settings
☒	☐ For hierarchical and complex designs, identification of the appropriate level for tests and full reporting of outcomes
☐	☒ Estimates of effect sizes (e.g. Cohen's *d*, Pearson's *r*), indicating how they were calculated

Our web collection on statistics for biologists contains articles on many of the points above.

Software and code

Policy information about availability of computer code

Data collection	To collect behavioral, histological and electrophysiological data, we used software packages and custom code (detailed in the Material & Methods section) written in Matlab 2015b (or more recent versions), Python 3.6.0 (or more recent versions), Octave, OpenGL, Patchmaster v2 x 32, and Fiji 2.1.0 (or more recent versions), and the following open source software programs and plugins: QuPath 0.2.3, SpikeGLX V20230101-phase30, PylonRecorder2, Bonsai V2.6.2, and BonVision V0.11.0, Psychtoolbox.
Data analysis	To analyse the data, we used custom code written in Matlab 2015b (or more recent versions), Python 3.6.0 (or more recent versions), Julia 1.11 and R Studio 1.1.383 (or more recent versions). The following packages/plugins were used: TrakEM2 (ImageJ plugin), StarDist (ImageJ plugin), R package lme4 and emmeans, Kilosort2, phy2, scikit-learn package (Python), DABEST (Python package), DeepLabCut V2.1.9 or newer, Fitmaster, Synaptosoft.

For manuscripts utilizing custom algorithms or software that are central to the research but not yet described in published literature, software must be made available to editors and reviewers. We strongly encourage code deposition in a community repository (e.g. GitHub). See the Nature Portfolio guidelines for submitting code & software for further information.

Data

Policy information about availability of data

All manuscripts must include a data availability statement. This statement should provide the following information, where applicable:

- Accession codes, unique identifiers, or web links for publicly available datasets
- A description of any restrictions on data availability
- For clinical datasets or third party data, please ensure that the statement adheres to our policy

The source data necessary to replicate key panels of figures 1-5 together with relevant code can be found here: https://doi.org/10.5061/dryad.q2bvq83xc

Research involving human participants, their data, or biological material

Policy information about studies with human participants or human data. See also policy information about sex, gender (identity/presentation), and sexual orientation and race, ethnicity and racism.

Reporting on sex and gender	n/a
Reporting on race, ethnicity, or other socially relevant groupings	n/a
Population characteristics	n/a
Recruitment	n/a
Ethics oversight	n/a

Note that full information on the approval of the study protocol must also be provided in the manuscript.

Field-specific reporting

Please select the one below that is the best fit for your research. If you are not sure, read the appropriate sections before making your selection.

☒ Life sciences ☐ Behavioural & social sciences ☐ Ecological, evolutionary & environmental sciences

For a reference copy of the document with all sections, see nature.com/documents/nr-reporting-summary-flat.pdf

Life sciences study design

All studies must disclose on these points even when the disclosure is negative.

Sample size	No methods were used to predetermine sample size. Sample sizes were set to match, or exceed, similar studies in the field. For behavioural studies we used cohorts of 14-116 animals; comparable experiments in mice have used 28 animals (https://doi.org/10.1016/j.cub.2016.06.006) or 10 animals (https://doi.org/10.1016/j.cub.2013.08.015). For c-Fos studies we used 21-66 animals; in published studies quantifying c-Fos in the context of innate behaviours, groups of 6-10 animals were used (https://doi.org/10.1038/s41586-018-0078-2). For Neuropixels recordings in behaving mice, we used 3-6 animals; comparable studies analysed 135 units obtained from 4 animals (https://doi.org/10.1073/pnas.2500321122) and we have previously published recordings from 6-8 animals in difficult to target regions (https://doi.org/10.7554/eLife.50697). Our optogenetic experiments were performed in cohorts of 5-13 animals; similar experiments targeted at modulating colliculus-mediated behaviours have been performed with groups of 7-8 animals (https://doi.org/10.1038/s41467-024-46460-z).
Data exclusions	For the optogenetics and electrophysiology experiment, animals were excluded if post-hoc immunohistochemistry showed no or little YFP staining in dPAG and/or incorrect fiber/electrode placement. We excluded optogenetic trials for which the animal moved less than 10 cm/s on average during the 0.5 s before laser trigger. For the smFISH-IHC analysis, we removed 7 sections that had poor staining intensity. We removed trials during the sweep-looming experiment when animals retreated to the hut during the sweeping stimulus (P. maniculatus, N=1; P. polionotus, N=3; P. leucopus, N=8), such that all animals were exposed to the subsequent looming stimulus. We removed trials for which animals did not show evidence of detecting the stimulus during the experiment to test for the effect of the presence/absence of a hut on the looming response (P. maniculatus, N=1/0; P. polionotus, N=1/2). All data exclusion criteria are explained in the Methods.
Replication	We performed all experiments successfully multiple times. In the Methods section "Animal Usage", a detailed description of the number of animals per experiment can be found. In the sections describing each experimental protocol, inclusion and exclusion criteria are described. Each included animal and/or recorded cell represents a replication, which is represented by displaying the individual data points or data traces for all types of experiments.
Randomization	The behavioral and electrophysiological experiments were based on observations, and no experimental groups were used. For the c-Fos, optogenetics and chemogenetics experiments, animals were randomly assigned to experimental groups (experimental vs. control).
Blinding	Investigators were not blind to experimental conditions. Most analyses in this study rely on quantitative and automated methods to analyse

Blinding	data. To determine if mice had detected a visual stimuli in Extended Data Figure 2, two independent observers manually scored videos, and only videos were included for which both observers determined that mice detected visual stimuli (for details, see Methods).

Reporting for specific materials, systems and methods

We require information from authors about some types of materials, experimental systems and methods used in many studies. Here, indicate whether each material, system or method listed is relevant to your study. If you are not sure if a list item applies to your research, read the appropriate section before selecting a response.

Materials & experimental systems

n/a	Involved in the study
☐	☒ Antibodies
☒	☐ Eukaryotic cell lines
☒	☐ Palaeontology and archaeology
☐	☒ Animals and other organisms
☒	☐ Clinical data
☒	☐ Dual use research of concern
☒	☐ Plants

Methods

n/a	Involved in the study
☒	☐ ChIP-seq
☒	☐ Flow cytometry
☒	☐ MRI-based neuroimaging

Antibodies

Antibodies used	rabbit anti-c-Fos antibody (Synaptic Systems, 226003), donkey anti-rabbit Alexa 647 antibody (Invitrogen, A31573), donkey anti-chicken Alexa 488 (Immuno Jackson, 703-545-155), chicken anti-GFP (Thermo Fisher, A-10262), HRP-labeled goat anti-rabbit antibody (PerkinElmer, NEF812001EA), rabbit anti-GFP (Thermo Fisher, A-11122)
Validation	The rabbit anti-c-Fos antibody was validated in tissue with known induction/expression patterns, and compared to alternative c-Fos antibodies. The manufacturer states that this antibody binds to human, mouse, rat, monkey, dog, pig and cow protein, and was validated by Western blot and immunohistochemistry. The chicken anti-GFP and rabbit anti-GFP antibodies were validated by the manufacturer, using relative expression analysis in Western blot.

Animals and other research organisms

Policy information about studies involving animals; ARRIVE guidelines recommended for reporting animal research, and Sex and Gender in Research

Laboratory animals	Peromyscus maniculatus bairdii (BW), Peromyscus polionotus subgriseus (PO), Peromyscus leucopus (LL), Mus musculus (C57Bl/6j). All animals were older than 8 weeks at time of testing.
Wild animals	No wild animals were used in this study.
Reporting on sex	Our study included both male and female mice, and approximately even numbers of males and females were used in all experiments. Sex was determined at weaning through inspection of the anogenital area. All behaviors and effects of optogenetic and chemogenetic manipulation were observed in both sexes, so that we decided to pool data across sexes. Sex was not considered further.
Field-collected samples	No field collected samples were used in this study.
Ethics oversight	Institutional Animal Care and Use Committee (IACUC) of Harvard University, and Animal Ethics Committee of KU Leuven.

Note that full information on the approval of the study protocol must also be provided in the manuscript.

Plants

Seed stocks	n/a
Novel plant genotypes	n/a
Authentication	n/a